Effect of carbonation treatment on fracture behavior of low-carbon mortar with recycled sand and recycled powder

Yuxiang Tang[a], Jianzhuang Xiao[a,b,*], Dianchao Wang[a], Mingzhong Zhang[c]

[a] *Department of Structural Engineering, College of Civil Engineering, Tongji University, Shanghai, 200092, PR China*

[b] *State Key Laboratory for Disaster Reduction in Civil Engineering, Tongji University, Shanghai, 200092, PR China*

[c] *Department of Civil, Environmental and Geomatic Engineering, University College London, London, WC1E 6BT, UK*

Abstract: This paper presents a systematic experimental study on the fracture behavior of low-carbon mortars with various contents of carbonated recycled sand and recycled powder (CRS and CRP). Three-point bending tests on pre-notched beams were performed to explore the load-induced fracture processes. Based on the strain and displacement fields measured using the digital image correlation technique, the evolution of the fracture process zone (FPZ) was studied qualitatively and quantitatively. Results indicated that the initial cracking toughness (K_{Ic}^{ini}), unstable fracture toughness (K_{Ic}^{un}) and fracture energy (G_f) of mortar reduced gradually with the increasing recycled sand (RS) content but kept relatively steady with the rising recycled powder (RP) dosage except for K_{Ic}^{ini}. Carbonation treatment could effectively improve the K_{Ic}^{ini} of mortar with low RP content and G_f with a high proportion of RS but had limited effect on K_{Ic}^{un}. A combination of the FPZ evolution characteristics and crack growth resistance curves suggested that the use of RS would increase microcracking in the stable crack growth stage and thus facilitate the connectivity of microcracks in the unstable fracture stage, while the use of RP mainly affected the crack initiation stage of cement paste in the mortar. The improvement of mortar fracture by CO_2 treatment of RS or RP also corresponded to these stages. Regarding fracture characteristics and carbon footprint, mortars with CRS and CRP could achieve a synergy of safety and low carbon and thus can be considered as low-carbon cementitious materials compared to normal mortar.

Keywords: Low-carbon mortar; Recycled sand; Recycled powder; Carbonation treatment; Fracture behavior; Fracture process zone.

* Corresponding author at: Department of Structural Eng., College of Civil Eng., Tongji University, Shanghai, PR China.
E-mail address: jzx@tongji.edu.cn (J. Xiao).

Nomenclature

f_{cu}, f_{st} and f_t	compressive strength, splitting tensile strength and tensile strength
L, D, S, and t	length, depth, span and thickness of the beam
a_0 and a_c	initial crack length and critical effective crack length
α_0 and α_c	ratios of initial crack length and critical effective crack length to beam depth
ε_{xx}	strain in x direction which is horizontal
P_{ini} and P_c	initial cracking load and peak load
CM(T)OD$_c$	critical crack mouth (tip) opening displacement at peak load
E	Young's modulus
C_i	initial compliance of the load-CMOD curve
h_0	thickness of the holder for clip gauge
K_{Ic}^{ini} and K_{Ic}^{un}	initial fracture toughness and unstable fracture toughness
m	mass of beam between the supports
W_0 and δ_0	area under the load–deflection curve and deflection at final failure
G_f	fracture energy
Δa	crack extension length
w_0	stress-free crack opening displacement

Acronyms

NS, RCA, (C)RS and (C)RP	natural sand, recycled coarse aggregate, (carbonated) recycled sand and (carbonated) recycled powder
RAC	recycled aggregate concrete
(C)RAM-25, 50 and 100	(carbonated) recycled aggregate mortar with 25%, 50% and 100% (C)RS
(C)FRAM-10, 20 and 30	(carbonated) RAM-100 with 10%, 20% and 30% of (C)RP

1. Introduction

As climate change becomes increasingly serious, most countries are conducting carbon neutrality initiatives. China aims to reach carbon peaking by 2030 and carbon neutrality by 2060 [1]. According to statistics, 30% of China's total carbon emissions was attributed to the production of building materials [2], indicating that green building materials are crucial for achieving carbon peaking and net zero targets. Cementitious materials are the most used and versatile building materials. The development and utilization of low-carbon cement and concrete are urgently needed. With the rapid growth of the construction industry, natural sand and gravel resources are increasingly scarce and expensive, and a great quantity of construction solid waste (mainly waste concrete) is generated [3]. Recycled concrete technology is an effective solution by converting waste concrete into recycled products for concrete preparation [4]. According to the particle size, recycled products can be divided into recycled powder (RP), recycled sand (RS), and recycled coarse aggregate (RCA). There are no uniform conclusions on the carbon reduction benefits of RAC [3]. On the one side, the use of recycled raw materials can avoid landfill of waste concrete and thus reduce the exploitation of natural mines, usage of cement and distance of transportation, which are conducive to carbon footprint reduction [5]. On the other side, the utilization of recycled raw materials generally weakens the strength and durability of concrete, causing an increase in cement consumption or pretreatment process to achieve the same service life, which is more likely to increase carbon emissions [6].

To reduce the negative impact of recycled products on concrete properties, different treatment methods have been proposed in recent years. For recycled aggregates (RAs), given the quality and quantity of adhered mortar, two pretreatment approaches are generally employed [7], namely removing or strengthening the adhered mortar. The former includes acid pre-soaking, thermal treatment, mechanical grinding, and microwave removal, while the latter contains polymer, pozzolan, accelerated carbonation and bio-deposition. For recycled powder, fineness improvement, heat treatment, alkali activation, CO_2 curing, and double mixing are the most common methods adopted to improve the performance of mortar and concrete with RP [8]. Among these methods, accelerated carbonation treatment receives wide attention since it can both improve the overall quality of recycled raw materials and permanently chemically convert CO_2 into minerals as follows [9, 10]:

$$Ca(OH)_2 + CO_2 \rightarrow CaCO_3 + H_2O \quad (1)$$

$$C\text{-}S\text{-}H + CO_2 \rightarrow CaCO_3 + SiO_2 \bullet nH_2O \quad (2)$$

Many efforts have been made to investigate the effects of CO_2 treatment of RAs and RP. It was reported that CO_2 treatment of RAs could enhance its physical properties, *e.g.*, increased apparent

density and reduced water absorption and crushing value [11]. With the enhancement of the quality of RAs, the prepared concrete materials also have certain performance improvements. For concrete using carbonated RCA, Xuan et al. [12, 13] found that CO_2 treatment of RCA could enhance the strength properties and durability of RAC since the microhardness of the old cement paste and new ITZ were enhanced, which is further characterized by using carbonated modelled RCA [14]. Constitutive relation is the link between materials and structural members. The uniaxial compressive stress-strain relationship of RAC using carbonated RCA and its strain-rate sensitivity was experimentally studied by Luo *et al*. [15] and Li *et al*. [16], respectively. In the case of reinforced recycled aggregate concrete, Liang *et al*. [17] and Peng *et al*. [18] reported that the utilization of carbonated RAs reduced the steel corrosion risk. For cement mortar utilizing carbonated RS, Zhang *et al.*[11] concluded that it had similar mechanical and shrinkage properties compared with natural mortar because of the enhanced microstructures of the original ITZ in RS and newly-formed ITZ in mortar. For cement paste employing carbonated RP, Lu *et al.* [19] suggested that it presented a lower porosity and a higher compressive strength due to the presence of a large amount of calcite in carbonated RP. Apart from the most concerned mechanical and durability properties, the effect of carbonation treatment on the fracture properties of recycled concrete is still unclear.

Since the fracture properties of cementitious materials are necessary for the safety and durability design of engineering structures [20], there are a large number of studies on the fracture behavior of RAC. For concrete employing untreated RCA, Ghorbel and Wardeh [21] reported that fracture energy and toughness decreased with increasing RCA contents, while Li *et al*. [22] found that the fracture energy of RAC was lower than NAC but fracture toughness kept unchanged. Besides fracture parameters, Guo *et al.* [23] evaluated the variation of the fracture process zone in RAC and reported that it was more localized and intense due to ITZ cracking. To improve the fracture properties of RAC, both the modification of raw materials and the mix design of concrete have been considered. Dilbas *et al.* [24] and Kazemian *et al*. [25] used optimized ball milling treatment and acid treatment to modify RCA, respectively. By designing with the particle packing method, Pradhan *et al*. [26] suggested that the fracture parameters of RAC were similar to that of normally designed NAC. Despite that the influence of RCA on concrete fracture behavior has been comprehensively studied, research on the influence of using RS and RP is still very limited. Akono *et al.* [27] investigated the fracture parameters and mechanisms of mortar with RS by employing nanoscale methods. Xiao *et al*. [28] found that the RAC mainly occurred transgranular or intergranular fracture with RCA or RS respectively, and RP made the fracture behavior of concrete less brittle. It is worth mentioning that RS and RP affect the cement mortar and paste respectively, so it is necessary to study their combine impact on cement-based materials from different scales. While few studies focused on the influence of the incorporation of RS and RP and the utilization of

carbonation treatment on fracture behavior of cement-based materials.

Therefore, this study aims to explore the influence of using RS and RP on the fracture behavior of cement-based materials and the improvement effect of carbonation treatment technology on the fracture property of mortar with RS and RP. To be specific, taking RS contents, RP contents and CO_2 treatment as the parameter variables, this paper studies the fracture behavior of cement mortar by performing three-point bending tests on center-notched beams. The complete load-displacement curves were recorded and various fracture parameters were extracted and analyzed. Then, through the strain and displacement fields measured by the digital image correlation (DIC) technique, the evolution of the fracture process zone (FPZ) was estimated qualitatively and quantitatively, respectively. By combining the FPZ characteristics and crack growth resistance curves, the potential fracture mechanism was clarified. Finally, the embodied carbon footprint of mortar with carbonated RS and RP was quantified to verify that it was low-carbon cement-based material, indicating that the carbonation treatment technology could achieve the synergism of safety and low carbon.

2. Experimental program

2.1 Raw Materials

In this study, river sand was used as natural sand (NS) and recycled sand (RS) was provided by a local construction and demolition (C&D) waste recycling plant through processing waste concrete, as displayed in Fig. 1. The maximum size of sand was 4.75 mm, and the fineness modulus of NS and RS was about 3.2 and 3.4, respectively. The synthetic grading was adopted to obtain similar grading curves of NS and RS (see **Fig. 2**) by referring to the limit value of the specification [29]. Based on the recommended methods in the standards [30, 31], the physical properties of sands were determined, as listed in **Table 1**. RS has lower apparent density but higher water absorption than NS due to the porous attached mortar.

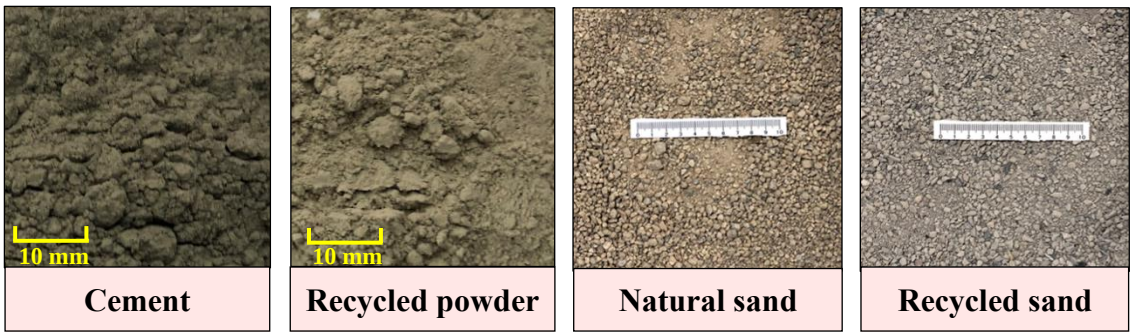

Fig. 1 Main raw materials for mortar preparation.

Ordinary Portland cement (P.O 42.5) was used as the main binding material. Recycled powder (RP) was adopted as a partial substitute for cement. The RP was prepared by grinding the dried RS into fine powder in a ball mill for about 30 minutes [32]. The particle size distribution of cement and RP determined using a laser particle size analyzer is presented in **Fig. 2**, indicating that RP

particles are obviously coarser than those of cement. More details about RP can be found in a previous study [32]. Clean tap water was used as mixing water and powdered polycarboxylate superplasticizer (SP) was added to improve the workability of mortar.

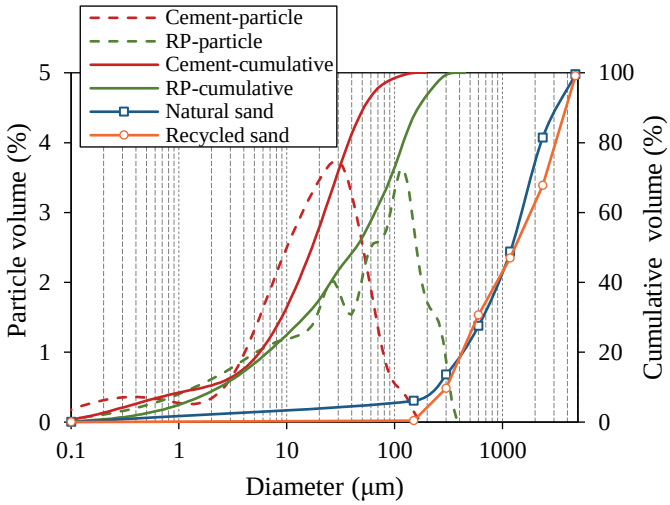

Fig. 2 Particle size distribution of binders and sand.

Table 1 Physical properties of sand used in this study.

Sands	Fineness modulus	Apparent relative density	Water absorption (%)	Water content (%)
NS	3.2	2.61	1.0	0.9
RS	3.4	2.24	13.3	6.6
CRS	3.4	2.30	10.9	5.4

After drying in an oven (60 ± 2°C) to constant weight, the RS and RP were carbonated for over 14d and 7d respectively in a carbonation chamber with a CO_2 concentration of 20 ± 2% and a relative humidity of 75 ± 5% [5]. After carbonation, the RS and RP were ground and evenly distributed, and then sprayed with phenolphthalein solution to see whether they were completely carbonated. The determined physical properties of CRS are listed in **Table 1**. It is noticed that the carbonation treatment increases the apparent density of RS and decreases the water absorption, which is due to the fact that $CaCO_3$ produced by the carbonation reaction can fill the pores on the adhered mortar of RS [5].

2.2 Mix proportions

In this study, the testing parameters were RS content (25%, 50% and 100% of the total aggregate), RP content (10%, 20% and 30% of the total binder) and modification treatment (untreated and CO_2-treated). The replacements of NS with RS/CRS and cement with RP/CRP were completed by the same volume and mass, respectively. With natural aggregate mortar (NAM, without RP and RS) as the reference mixture, a total of thirteen mixtures with the water-to-binder ratio of 0.45 were considered, as listed in **Table 2**. Extra mixing water was added to reduce the effect of the high water-absorption of RS/CRS. As RS was not completely saturated during mixing [33], the extra water was

taken as 70% of RS/CRS water-absorption [34, 35]. The SP content of each mixture was adjusted to gain close and preferable workability, as assessed by the flow table test. The corresponding flow value was about 210 ± 30 mm, as listed in Table 2. The addition of RP/CRP reduces the amount of SP required for similar fluidity, implying that it can improve the workability of mortar.

Table 2 Mix proportions and flow values of mortar.

Mix ID	Mix proportions (kg/m^3)									Flow values
	Cement	RP	CRP	NS	RS	CRS	Water	Extra water	SP	(mm)
NAM	675.6	-	-	1229.6	-	-	304.0	-	1.35	240
RAM-25	675.6	-	-	922.2	277.0	-	304.0	7.4	1.35	240
RAM-50	675.6	-	-	614.8	552.3	-	304.0	15.0	1.35	225
RAM-100	675.6	-	-	-	1104.6	-	304.0	29.9	2.36	225
CRAM-25	675.6	-	-	922.2	-	283.8	304.0	6.6	1.35	220
CRAM-50	675.6	-	-	614.8	-	567.5	304.0	13.0	1.35	210
CRAM-100	675.6	-	-	-	-	1136.7	304.0	26.0	1.35	200
FRAM-10	608.0	67.6	-	-	1104.6	-	304.0	26.0	1.22	205
FRAM-20	540.5	135.1	-	-	1104.6	-	304.0	26.0	0.81	225
FRAM-30	472.9	202.7	-	-	1104.6	-	304.0	26.0	0.71	210
CFRAM-10	608.0	-	67.6	-	-	1136.7	304.0	26.0	0.91	210
CFRAM-20	540.5	-	135.1	-	-	1136.7	304.0	26.0	0.81	200
CFRAM-30	472.9	-	202.7	-	-	1136.7	304.0	26.0	0.71	190

Notes: NAM is natural aggregate mortar. RAM-25, 50 and 100 is recycled aggregate mortar with RS content of 25%, 50% and 100%, respectively. CRAM-25, 50 and 100 is CO_2-treated recycled aggregate mortar with CRS content of 25%, 50% and 100%, respectively. FRAM-10, 20 and 30 is full-recycled-aggregate mortar with RP content of 10%, 20% and 30%, respectively. CFRAM-10, 20 and 30 is CO_2-treated full-recycled-aggregate mortar with CRP content of 10%, 20% and 30%, respectively.

2.3 Specimen preparation

The preparation process of the mortar mixture was based on a two-stage mixing method [36]. Firstly, the sand and half of the required water were mixed in the mixer for 60 s. Binders and SP were then added and stirred for 30 s. Finally, the other half of the water was poured, and the mixing time was taken as 120 s. The fresh mixture was poured into various plastic molds and compacted using a vibration table. For each mixture, 6 cubes (40 ×40 ×40 mm) and 4 prisms (40 ×40 ×160 mm) were cast. The specimens were cured in a tank filled with saturated calcium hydroxide solution to prevent the leaching of calcium hydroxide, which would affect the hydration process of cement and thus the mortar strength [37, 38]. Each prism was sawn a notch with a depth of 12 mm and a width of 3 mm in the center position and then loaded in nearly 60 d. The initial notch to beam depth ratio ($\alpha_0 = a_0/D$) was 0.3. The cubes were used to determine the compressive and splitting tensile strength (f_{cu} and f_{st}) of mortar as per the standards [37, 39].

2.4 Testing method

Fig. 3 illustrates the three-point bending tests on the center-notched beam performed using an MTS machine. The beam span to depth ratio (*S*/*D*) was 2.5. The crack mouth opening displacement (CMOD) was measured by a clip gauge placed at the bottom of the specimen. The initial cracking load (P_{ini}) was monitored by two strain gauges with a distance of 10 mm as per the RILEM standard [40]. The length and width of the strain gauge were 5 mm and 3 mm, respectively.

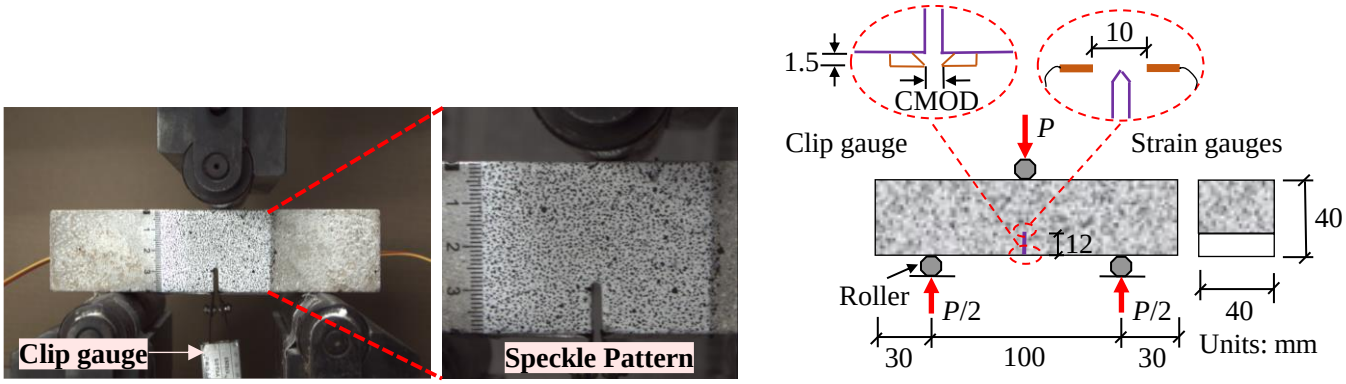

(a) (b)

Fig. 3 Schematic illustration of three-point bending test: (a) Front view; (b) rear view.

A digital camera was used to take the images during the loading process to monitor the deformation field using DIC. To apply this technology, it was first necessary to make speckles on the observation area. After polishing and cleaning the specimen surface, the white paint was sprayed to generate a white background, and then the black marker was used to artificially make uniformly-distributed dots, as displayed in **Fig. 3** a. The scale of the measurement was about 10 pixel/mm and the speckle size was about 5 pixels. The subset size and step size were taken as 19 pixels and 7 pixels, respectively. More details on the use and post-processing of DIC technology can be found in Ref. [41].

For tests, the sample was firstly preloaded with a load of 20 N to reduce the impact of possible looseness and measure reliable data. To achieve quasi-static loading for detecting stable crack growth, the fracture test was carried out at a constant loading rate of 0.02 mm/min using the displacement control of the loading point (*i.e.*, the displacement of the MTS crosshead) after some preliminary experiments. The mid span deflection δ of the notched beam was taken as the displacement recorded by the MTS sensor. The applied load *P* and CMOD were also automatically recorded by the MTS machine while the data of strain gauges was collected via a static strain collecting device.

3. Experimental results

3.1. Compressive and splitting tensile strengths

Fig. 4 presents the compressive strength (f_{cu}) and splitting tensile strength (f_{st}) of mortar specimens

with various RS and RP contents. As seen in **Fig. 4**a, with the increase of RS and RP contents, the f_{cu} of mortar drops continuously. The similar reduction can be found in many existing test results for mortar incorporating with RS [42] or RP [43]. For the mortar using RS, this is mainly due to (1) the need of additional water, increasing the ratio of effective water-to-binder in the mixes [44], and (2) the porous adhered cement paste in RS (even pure old cement paste), resulting in poor aggregate strength and multiple ITZ [45]. While for the mortar incorporating RP, the reduction of f_{cu} can be mainly attributed to the decreasing of hydration products with the lower clinker content [8].

From **Fig. 4**a, the f_{cu} of CO_2-treated mortars is about 1.3-10.5% higher than that of untreated mortars especially when the RS content is 100%. As less additional water is used in CRAM to meet the similar flowability to RAM, the effective water-to-binder ratio of CRAM is reduced, which contributes to the larger f_{cu} of CRAM [46]. The higher content of CRS in CRAM leads to less additional water in the mixture, which results in a more significant increase in strength. As the RP content increases, the effect of CO_2 treatment on improving f_{cu} is diminished from 8.1% to 4.0%. A similar phenomenon was reported by Lu *et al*. [19], who found that cement pastes with 10–20% CRP increased f_{cu} but those with 30% CRP decreased f_{cu}. They pointed out the improved strength with CRP was due to that: (1) the calcite in CRP provided a lot of additional nucleation and played a filler role; (2) calcium aluminate mono-carbonate products were formed. If the RP content is too high, the weakening effect of f_{cu} caused by less hydration products becomes more pronounced.

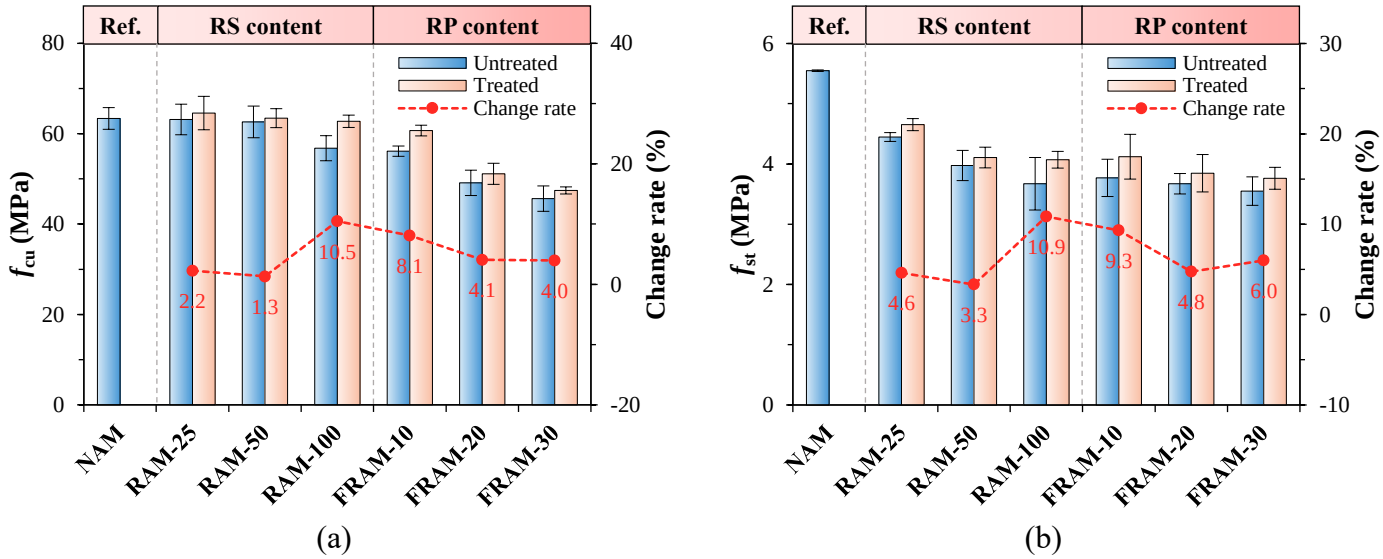

Fig. 4 Mechanical properties of the mortars with different contents of RS and RP: (a) Compressive strength; (b) splitting tensile strength.

As seen in **Fig. 4**b, the f_{st} of mortar has a similar variation tendency as the f_{cu} among different mix proportions. It decreases almost continuously with increasing use of RS and RP. Also, the f_{st} of mortar with CRS/CRP was enhanced to a certain extent (about 3.3-10.9%) as compared to that using the same amount of RS/RP. The levels of increase are higher under the conditions of a high

replacement ratio of RS and a low replacement ratio of RP. Overall, the carbonation treatment of RS/RP improves the strength properties of cement mortar incorporating RS/RP.

3.2. Load-CMOD curves

Fig. 5 shows the *P*-CMOD curves of mortar with different types and contents of RS and RP. It can be observed that the utilization of recycled materials has a limited effect on the shape of curves. The relationship between *P* and CMOD reflects the typical quasi-brittle fracture behavior and can be roughly divided into three stages. At the early loading level, the specimen is nearly in the linear elastic deformation stage and the strain ε at the notch tip increases with the loading (see Fig. 6). As the initiation of cracking, nonlinear deformation begins to appear, and ε reaches its maximum value. The load at this time (about 811 N for this FRAM-10 sample) can be regarded as the crack initiation load P_{ini} [40]. After that, the nonlinear deformation rises and the crack is in the stage of stable propagation. The ε of mortar near the notch tip decreases continuously because of the release of strain energy after cracking. When the load reaches the peak value (P_c), the accumulated strain energy is released rapidly and the crack propagates unstably, which is reflected in the sharp decline of the curve.

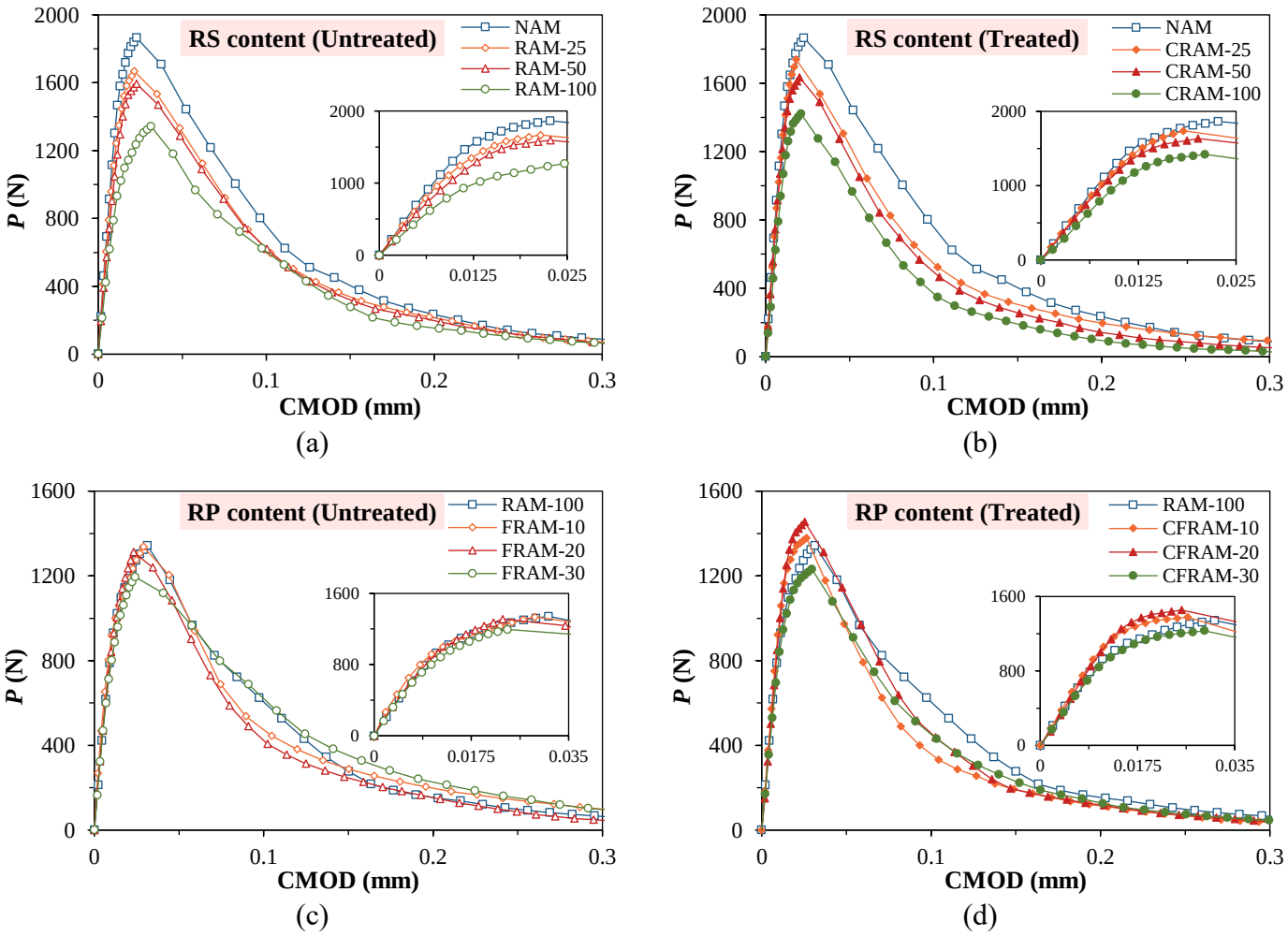

Fig. 5 Load-CMOD curves of the mortars with different contents of RS and RP: (a) Untreated RS content;

(b) CO_2-treated RS content; (c) untreated RP content; (d) CO_2-treated RP content.

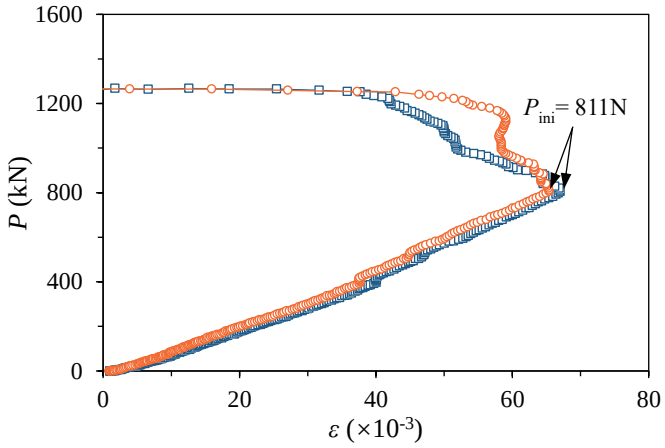

Fig. 6 Typical curves of applied load *P* versus the strain *ε* at the notch tip.

As shown in **Fig. 5**a and b, with the increase of RS/CRS content, the slope of the initial linear segment and peak load decreases significantly, and the reduction becomes smaller for the mortar using CRS. Except the case of 30% RP, there is a limited effect on them with the use of RP (see **Fig. 5**c), and they are improved even beyond the control group without RP after carbonation treatment (see **Fig. 5**d). **Fig. 7** presents the P_{ini} (measured by strain gauges) and P_c of mortar. With the increase of RS/CRS content up to 100%, the P_{ini} and P_c of mortar decrease by about 31.2%/25.3% and 25.2%/20.7%, respectively. This indicates that the resistance to crack initiation and bending bearing capacity of mortar decrease with the use of RS but the adverse effect can be weakened by employing carbonation pre-treatment. The utilization of RP reduces the P_{ini} of mortar at all RP dosage levels (about 14.1-21%), but reduces the P_c of mortar only at 30% RP dosage level. Carbonation treatment of RP can increase two loads of mortar containing RP, especially at 10% and 20% dosage RP levels.

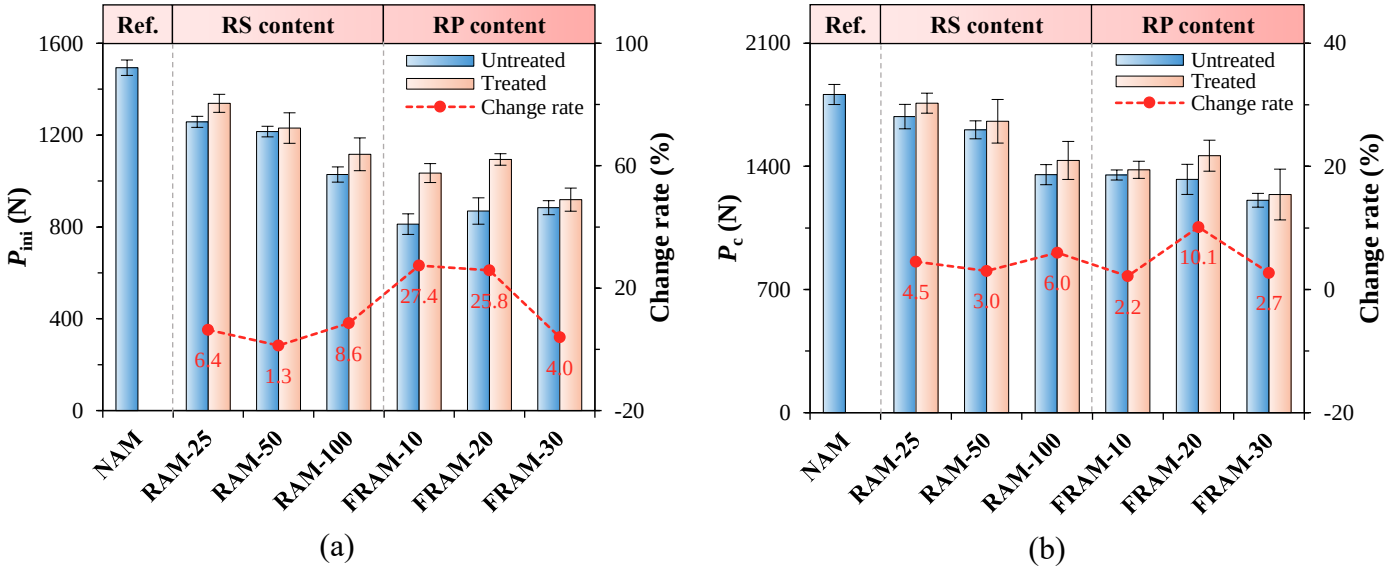

Fig. 7 Initial cracking and peak load of the mortars with different contents of RS and RP: (a) Initial cracking load; (b) peak load.

3.3. Critical crack propagation

Crack propagation at peak load (*i.e.*, critical crack propagation) is often used to assess the deformability of cementitious materials. It mainly includes critical crack length (a_c, in crack extension direction) and critical crack tip opening displacement ($CTOD_c$, in crack opening direction). For a_c, based on linear asymptotic superposition assumption, it can be estimated by the following expression according to the Double-*K* Fracture Model [40]:

$$a_c = \frac{2(D+h_0)}{\pi}\arctan\sqrt{\frac{tE}{32.6(P_c+0.5mg)}\mathrm{CMOD}_c - 0.1135} \quad (3)$$

in which *S*, *D* and *t* are the span, depth and thickness of the specimen, respectively. h_0 is the thickness of the holder of the clip gauge, which is equal to 1.5 mm in this study. $CMOD_c$ is the CMOD at the peak load. *m* is the mass of the specimen between the supports, and *g* is the gravity acceleration (9.81 m/s^2). Young's modulus *E* can be determined as follows.

$$E = \frac{1}{tC_i}[3.70 + 32.60\tan^2(\frac{\pi}{2}\frac{a_0+h_0}{D+h_0})] \quad (4)$$

where C_i is the initial compliance of the load-CMOD curve.

For $CTOD_c$, the calculation formula based on linear elastic fracture mechanics theory in the Two Parameter Fracture Model is as follows [47].

$$\mathrm{CTOD}_c = \mathrm{CMOD}_c \times \left\{\left(1-\frac{a_0}{a_c}\right)^2 + \left(1.081-1.149\frac{a_c}{D}\right)\left[\frac{a_0}{a_c} - \left(\frac{a_0}{a_c}\right)^2\right]\right\}^{1/2} \quad (5)$$

Fig. 8a and b show the calculated a_c and $CTOD_c$ of mortar, respectively. As seen in **Fig. 8**a, the a_c of different mortar mixtures is about 17.9 mm. Similar results were reported in the study by Xiao *et al*. [28], who found that the a_c of concrete almost did not change with the addition of RCA, RS and RP. After the carbonation treatment of the recycled materials, the a_c of mortar is reduced by about 1.2-7.3%. As illustrated in **Fig. 8**b, incorporating 100% RS makes the $CTOD_c$ of mortar increase markedly and using a growing number of RP makes it decrease continuously. This phenomenon was also observed in fully recycled aggregate concrete [28], in which only RCA was added relative to the proportion in this study. It can be observed from **Fig. 8**b that carbonation treatment of RS/RP reduces the $CTOD_c$ of mortar, except for FRAM-30. These indicate that the carbonation treatment has a limiting effect on the critical crack expansion of mortar containing RS/RP, which can be explained by the results of elastic modulus that reflect the deformation ability of the material. **Fig. 9** illustrates the estimated results of the *E* of mortar. It can be found that the *E* of mortar decreases gradually with the use of an increasing number of recycled materials, and CO_2 pre-treatment can improve the *E* of mortar (about 2.0-8.3%). The enhancement effect is close to the research result by Luo *et al*. [15], who reported that the increase of *E* caused by carbonation treatment of RCA was about 0.7%-5.8% under the replacement ratios from 30% to 100%. As the modulus of elasticity increases, the deformation ability of mortar becomes weaker, resulting in a smaller crack opening

displacement [24].

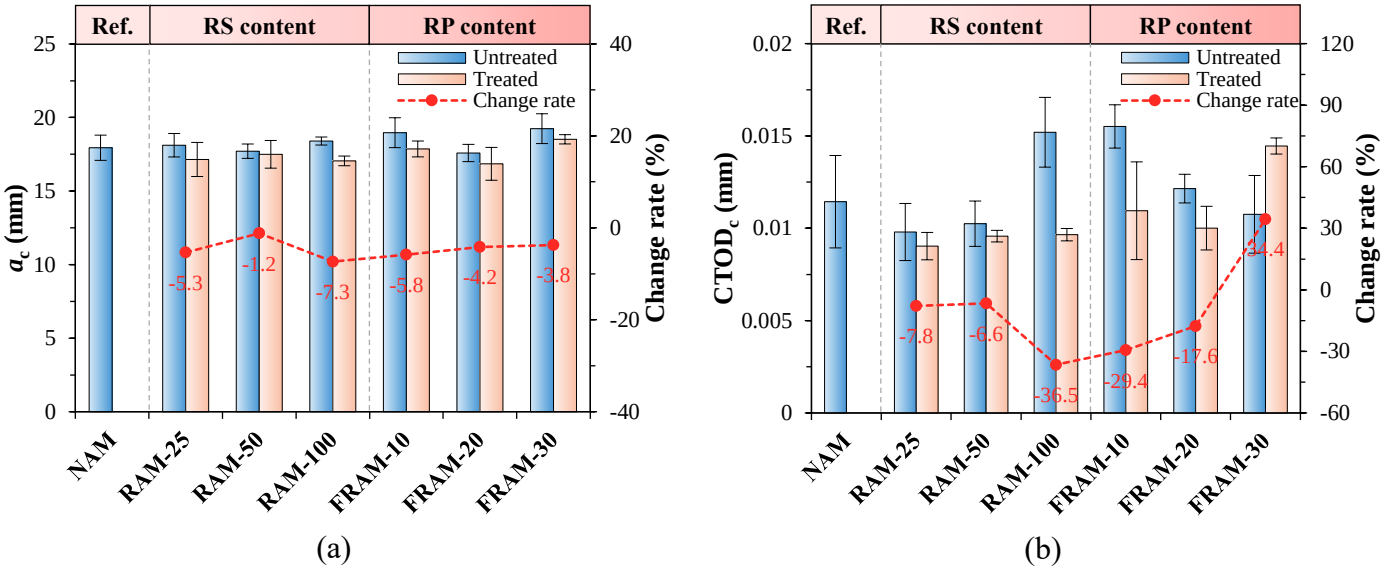

Fig. 8 Critical crack propagation of the mortars with different contents of RS and RP: (a) critical crack length; (b) $CTOD_c$.

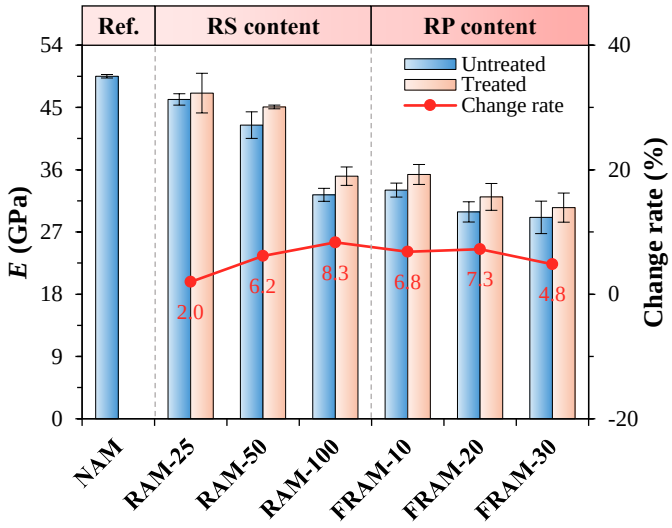

Fig. 9 Young's modulus of the mortars with different contents of RS and RP.

3.4. Double-K fracture toughness

As an important parameter to evaluate the fracture property of cementitious materials, fracture toughness K represents the load-induced fracture resistance of materials. The classical Double-K Fracture Model [48] was used in this study. In this model, the fracture process of materials is divided into three periods by initial cracking toughness K_{Ic}^{ini} and unstable fracture toughness K_{Ic}^{un}: 1) initial cracking ($K = K_{Ic}^{ini}$), 2) stable crack propagation ($K_{Ic}^{ini} < K < K_{Ic}^{un}$) and 3) unstable failure ($K_{Ic}^{un} < K$).

The K_{Ic}^{ini} can be obtained by putting the P_{ini} and a_0 of the specimen into the following equation [48]:

$$K_{Ic}^{ini} = 1.5\frac{(P_{ini} + 0.5mg)S}{D^2 t}\sqrt{a_0}F(\alpha_0) \quad (6)$$

where $F(\alpha_0)$ is the geometric shape function determined as follows.

$$F(\alpha_0) = \frac{1.99 - \alpha_0(1-\alpha_0)(2.15 - 3.93\alpha_0 + 2.7\alpha_0^2)}{(1+2\alpha_0)(1-\alpha_0)^{3/2}} \quad (7)$$

The K_{Ic}^{un} of mortar can be calculated by replacing P_{ini} and a_0 with P_c and a_c in Eqs (6) and (7). **Fig. 10**a and b present the determined K_{Ic}^{ini} and K_{Ic}^{un} of each group of mortar, respectively. As seen from **Fig. 10**a, with the increase of RS content from 25% to 100%, the K_{Ic}^{ini} of mortar decreases from 0.581 MPa.m$^{1/2}$ to 0.475 MPa.m$^{1/2}$, which is about 15.8-31.1% lower than that of NAM (about 0.689 MPa.m$^{1/2}$). This result is similar to the existing experimental study [28], where the K_{Ic}^{ini} of concrete with 100% RS decreased by 38.6% compared with that of normal concrete. It is due to the loose ITZ [27], larger porosity [44] and lower strength of mortar with RS causes it to be more sensitive to cracking and reduces its ability to resist crack initiation. Carbonation treatment of RS can correspondingly improve these adverse effects, resulting in the enhancement of the K_{Ic}^{ini} of the prepared mortar (about 1.3-8.6%). The K_{Ic}^{ini} of FRAM with 10-30% RP, about 0.375-0.409 MPa.m$^{1/2}$, is approximately 13.9-21.1% lower than that of RAM-100. This result seems different from the finding reported by Xiao *et al*. [28], who found that the influence of 10-30% RP content was limited relative to the obvious weakening effect of RS on the K_{Ic}^{ini} of concrete. The reason may be that for the concrete with coarse aggregate, the matrix that determines crack initiation is cement mortar, while for the mortar with fine aggregate, it is cement paste, which is the scale of direct influence of RP as a supplementary cementitious material. This view can be further verified by the fact that the K_{Ic}^{un} values of mortar remain almost steady with the increase of RP content (see **Fig. 10**b), which is consistent with the unchanged K_{Ic}^{ini} values of the concrete incorporating different RP [28]. After the carbonation treatment of RP, the K_{Ic}^{ini} of mortar has a remarkable improvement at the content of 10-20% (about 25.8-27.3%).

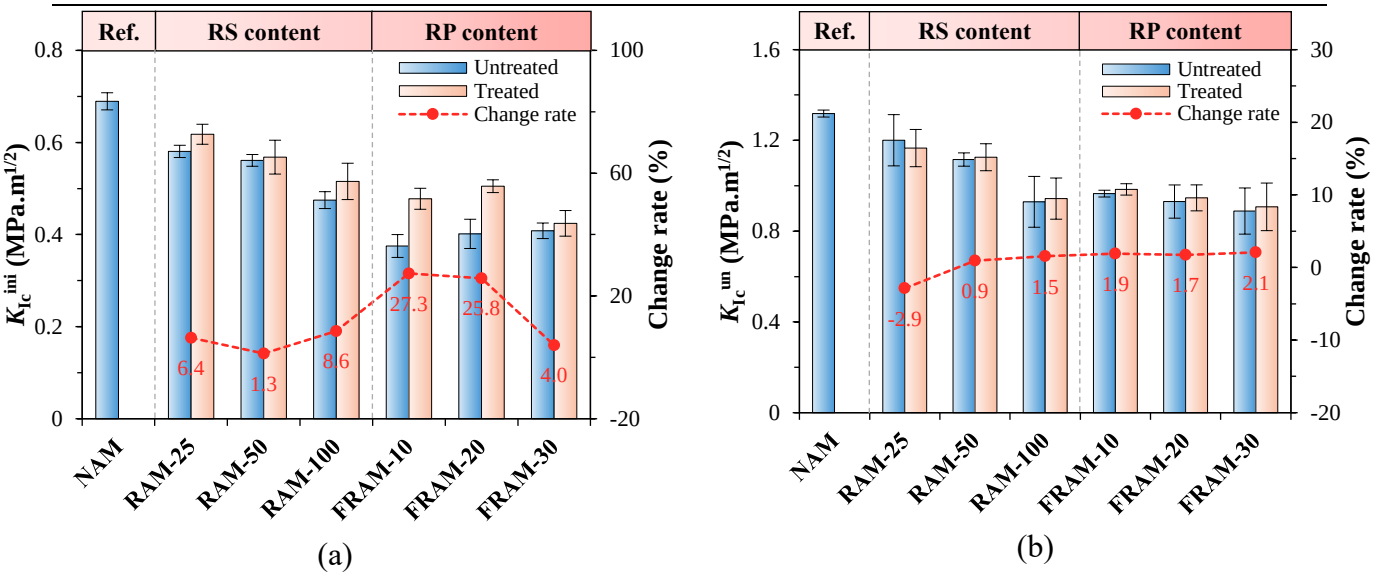

Fig. 10 Double-*K* fracture toughness of the mortars with different contents of RS and RP: (a) Initial cracking toughness; (b) unstable fracture toughness.

It can be seen from **Fig. 10**b that, the K_{Ic}^{un} values decrease by about 8.9-29.5%, with the RS content varying from 25% to 100%. The reduced K_{Ic}^{un} agrees well with the observation by Akono *et al*. [27], who found an 8% decrease in K_{Ic}^{un} for RAM by adopting nanoscale mechanical characterization methods. Accelerated carbonation technology slightly improves the K_{Ic}^{un} of mortar mixed with recycled materials (about 0.9-2.1%), except for RAM-25. In the study of Kazemian *et al*. [25], the K_{Ic}^{un} of concrete containing RCA was not obviously affected by the acid and Calcium Metasilicate slurry treatment of aggregates. While in the test of Dilbas *et al* [24], the K_{Ic}^{un} value of RAC could be significantly improved to be close to that of natural aggregate concrete by employing an optimized ball milling method to remove adhered mortar of RCA. In general, for this test study, the critical crack propagation resistance of mortar is reduced by using RS, while it is less affected by the addition of RP and the employment of carbonation treatment.

3.5. Fracture energy

As another significant fracture parameter, the fracture energy G_f reflects the energy consumed by the crack propagation per unit area [49], and can be obtained from the area under the entire load-displacement curve (W_0) as follows [50].

$$G_f = \frac{(W_0 + mg\delta_0)}{(D - a_0)t} \tag{8}$$

where δ_0 is the deflection when the final failure occurs.

Fig. 11 shows the determined G_f of the mortar specimens. Like the variation of K_{Ic}^{un}, the G_f values of RAM decrease with increasing RS contents while keeping stable with increasing RP contents. With RS contents varying from 25% to 100%, the G_f of mortar is about 13.9-37.8% lower than that of NAM. This finding agrees with previous results regarding the fracture energy of RAC [21, 22,

51], in which the G_f of concrete decreased with the increase of the replacement ratio of RCA. The reduced energy consumption for crack propagation may be due to less branching and meandering of cracks [22], and the weaker bridging effect of aggregate interlock [25], which are caused by the multiple ITZ and initial damage of recycled aggregates [28]. In addition, considering that some of RS is pure old cement matrix without part of river sand, the energy consumed by its cracking is undoubtedly decreased.

It can be seen from **Fig. 11** that, the G_f of mortar using CO_2-treated recycled materials is higher than that of mortar using untreated recycled materials. The improvement rate increases with increasing RS content (about 8.3-14.0%) and decreases with increasing RP content (about 5.1-7.8%), which is consistent with the strength improvement effect among different RS/RP contents (see **Fig. 4**). Kazemian *et al*. [25] reported the improved G_f of concrete with treated RCA and attributed it to the enhancement of the interface bonding between paste and aggregate.

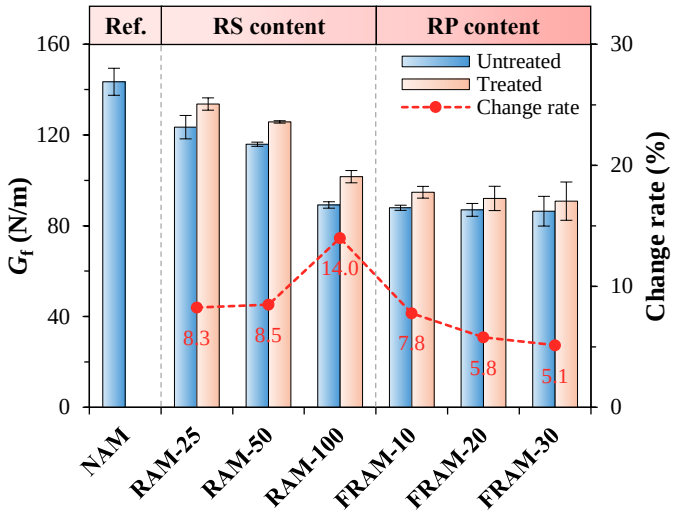

Fig. 11 Fracture energy of the mortars with different contents of RS and RP.

3.6. Fracture process zone evolution

The energy dissipation during the fracturing process is concentrated in the fracture process zone (FPZ), which is a damage zone with many fracture toughening mechanisms, including microcracking, crack deflection, branching and aggregate bridging [52]. The geometry of FPZ can be visualized by the measured surface strain field [53-56]. To employ it, it is necessary to specify the strain threshold to eliminate the irrelevant noise [56, 57]. The maximum tensile strain was approximately taken as the result of dividing tensile strength f_t by E, and the value of f_t was taken as 0.9 times of f_{st} [58]. In this study, the FPZ region was defined as the extent to which the strain in the x direction (ε_{xx}) exceeded the estimated maximum tensile strain.

To analyze the complete fracture process of mortar, four typical loading levels were selected, as shown in **Fig. 12**, including pre-peak 60% P_c, peak load, post-peak 60% P_c and post-peak 20% P_c. **Fig. 13** illustrates the strain fields above the notch of five group specimens, including NAM, RAM-

100, CRAM-100, FRAM-20 and CFRAM-20. The FPZ can be considered as the area of strain localization [55-57, 59]. To better compare the FPZ evolution of different mortars, the same strain interval was used at each loading stage. It can be seen from the figure that the evolution tendency of the mortar FPZ is similar among different groups despite the size of the localized zone and magnitude of strain. At the loading stage about pre-peak 60% P_c, the main crack initiates from the center-notch tip where the stress concentration and some microcracks occur. At the peak load, the main crack propagates in a stable manner and its shape is tortuous as per randomly distributed aggregates. After that, the main crack develops rapidly. When the load drops to about 20% P_c, the FPZ is fully developed (discussed below) and presents an irregular narrow strip. Comparing the fully-developed localized zone of different groups of specimens, it can be found that the width of the localized zone is larger in mortars with RS or RP compared with NAM, whereas the width is reduced after using accelerated carbonation technology.

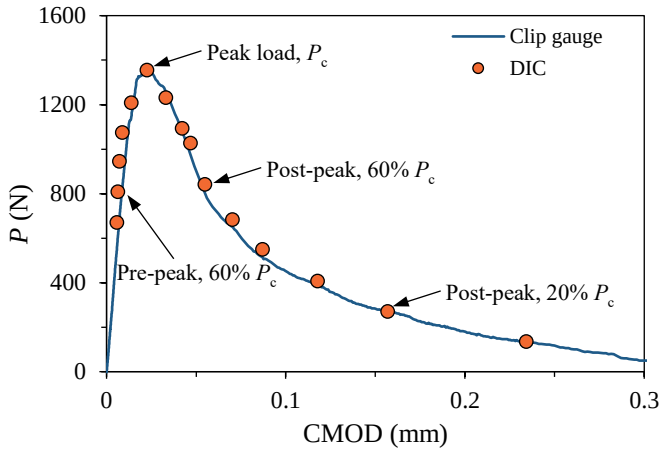

Fig. 12 A typical comparison of *P*-CMOD curves measured by clip gauge and DIC.

It is noticed that the strain field can only provide a qualitative description on the FPZ evolution. Considering that the strain is calculated based on the reference length, the discontinuity of the cracking region can cause deviations [53, 55, 57]. To quantitatively analyze the FPZ evolution, the displacement field obtained by DIC was employed in this study. Taking a specimen of CFRAM-20 as an example, the DIC measured x-displacement (u) at the loading level of post-peak 20% P_c is demonstrated in **Fig. 14**. The crack opening displacement (COD) can be determined by the amplitude of horizontal displacement jump and the crack tip can be defined as the location at which the jump disappears [59-61]. As seen in **Fig. 14**a, the crack mouth (y = 0 mm) and tip (y = 12 mm) opening displacement (CMOD and CTOD) and the crack extension length Δa can be estimated by the DIC measured displacement field. **Fig. 14**b shows the locally amplified and planarized displacement distribution above the notch. As can be seen, an obvious displacement jump occurs around the center-notch, caused by the crack opening. Away from the center position, the displacement distribution becomes continuous since there is still in the elastic state [53, 62]. The COD can be obtained by subtracting u at both sides of the crack face. The CTOD is equal to about 0.084 mm at

this loading level. As the distance from the notch tip increases, the COD decreases gradually. The crack tip can be considered as the position where the whole displacement keeps continuous, which is about 37 mm (*i.e.*, a = 37 mm and Δa = 25 mm). By comparing the CMOD measured by DIC with the result measured by clip gauge (see **Fig. 12**), excellent consistency can be observed, thus validating the accuracy of the displacement field measured by DIC.

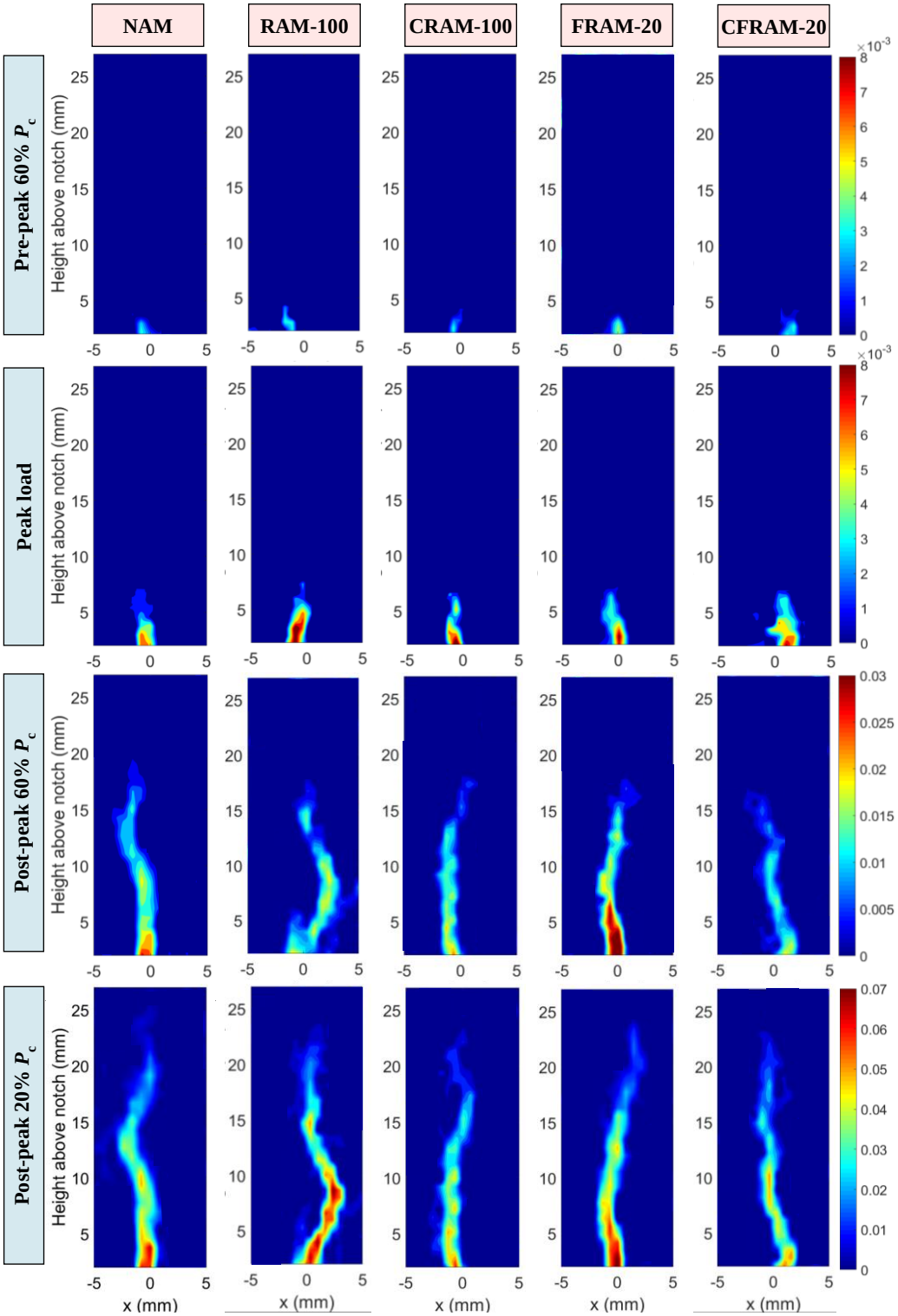

Fig. 13 Strain localization zones of the mortars with different contents of RS and RP at different loading stages.

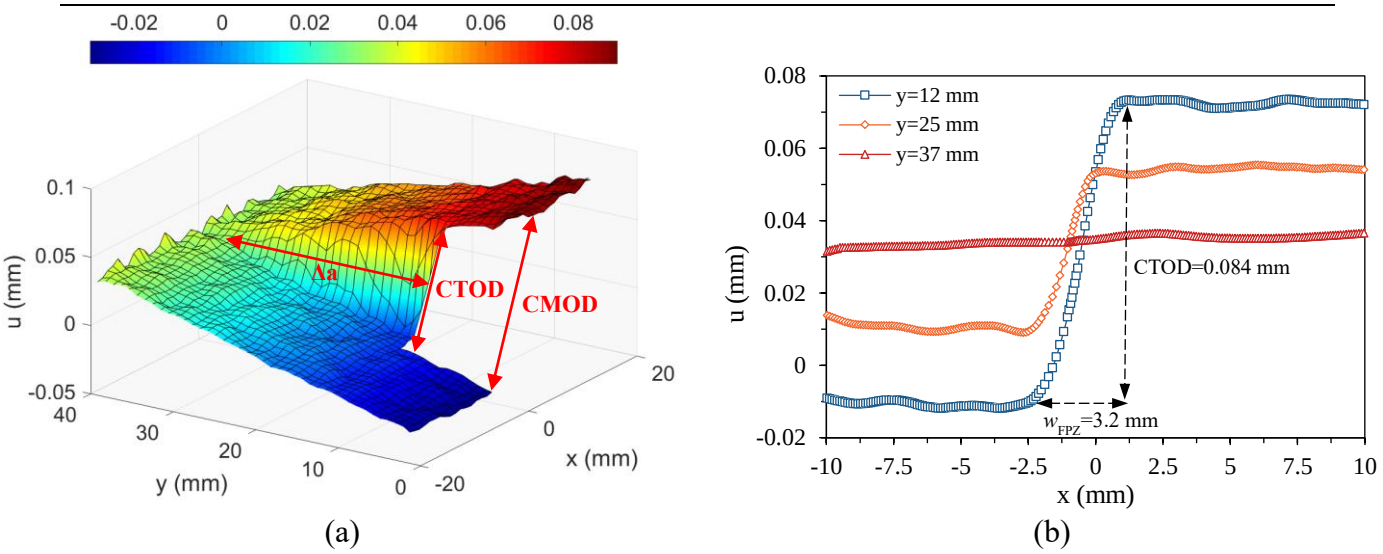

Fig. 14 Determination of crack propagation from the DIC measured *x*-displacement field: (a) 3D view; (b) plane view.

Fig. 15 plots the relationship between the DIC measured crack opening (CTOD) and growing (a) of each group of specimens. It is noteworthy that each specimen could only select the DIC analysis step according to the gradient of about 10% P_c (see **Fig. 12**) as far as possible, considering that some specific loading stages might not be captured by the camera. Before the peak load, the CTOD is small, which is mainly caused by microcracking, and the crack expands slowly. When the load reaches its peak, the mean CTOD and a of mortar with different RS contents are about 0.007-0.014 mm and 18.6-20.9 mm, respectively. For the mortar with different RP contents, two values are about 0.007-0.018 mm and 18.9-21.0 mm, respectively. These results are in good agreement of the previously calculated $CTOD_c$ and a_c (see **Fig. 8**), which indicates the applicability of the existing fracture mechanics formula for normal cementitious materials is not affected by the employment of recycled materials. After the peak load, the crack expands rapidly in both the opening direction and the growth direction. The rear of FPZ (*i.e.*, the tip of traction-free crack) maintains at the notch tip and does not move forward until the FPZ is fully developed. In this case, the FPZ length is equal to the crack extension length Δa. In the fictitious crack model [63], the cohesive stress of FPZ can be expressed as a function of crack opening displacement (*i.e.*, cohesive softening law). The rear of the fully-developed FPZ can be estimated by the position where the CTOD reaches the stress-free crack opening displacement w_0 [53, 64-66]. Given that the coefficient of cohesive law seems to be less affected by the incorporation of recycled aggregates [21], the value of w_0 was taken as 3.6 G_f/f_t [67] in this study. As seen from **Fig. 15**a and b, when the FPZ is fully developed, the values of CTOD and a are 0.080-0.115 mm and 35-37.6 mm for mortar with various RS contents and 0.082-0.106 mm and 35-36.9 mm for mortar with various RP contents. Then, since the crack tip has reached around the specimen boundary, the crack is restrained along the extension direction, and propagates mainly along the opening direction.

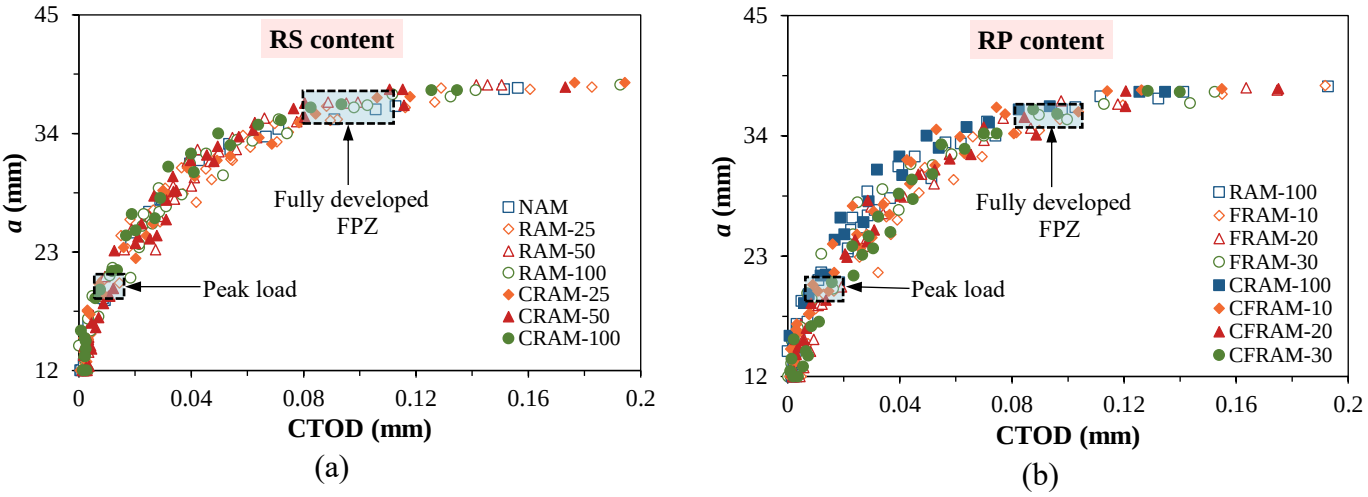

Fig. 15 Relation between the CTOD and crack length *a* measured by DIC: (a) RS content; (b) RP content.

The length of FPZ (l_{FPZ}) is an essential geometric parameter as per the cohesion distribution in the FPZ depends on its length [59, 68]. In this study, the l_{FPZ} of mortar was determined based on the extent of displacement jump in the direction of crack-extension, as discussed before. To evaluate the variation of the l_{FPZ} in different groups of specimens, the relations between it and the normalized load (P/P_c) and crack-extension $(a-a_0)/(D-a_0)$ are shown in **Fig. 16**. Regardless of the type, dosage, treatment of recycled materials, the shape of these curves is generally similar. At the peak load, the l_{FPZ} is about 0.24-0.32 of the ligament depth (*i.e.*, D-a_0). When the load decreases to about 0.20-0.32 P_c, the FPZ is completely developed and achieves its maximum length, which is around 0.84-0.92 of the ligament depth. After the FPZ is fully developed, the l_{FPZ} decreases with crack propagation. It may be attributed to the boundary effect of the specimen as the residual ligament is not long enough, thus the crack opening dominates the crack propagation. Similar phenomena were also reported in previous studies [54, 55], where the maximum l_{FPZ} was about 0.75-0.90 and 0.86-0.92 of the ligament depth for normal concrete [55] and manufactured-sand recycled aggregate concrete [54].

In addition to the cohesive stress distributed on the FPZ length, the crack tip blunting caused by the FPZ width (w_{FPZ}) can also lead to the quasi-brittle and elastic-plastic fracture behavior of cementitious materials [69]. The value of w_{FPZ} can be determined from the horizontal distance between the start and end of the displacement jump [57] as seen in Fig. 14, which is about 3.2 mm at this loading stage. By comparing the results of y = 12 mm and y = 25 mm, it can be found that w_{FPZ} decreases with the distance far from the notch. Generally, the reduction of w_{FPZ} becomes prominent beyond a certain crack extension [59]. Given that the setting of parameters related to the subset affects the boundary range of DIC measurement [41], the w_{FPZ} at a location 2 mm above the notch was taken to facilitate a comparison of the different mortars. The FPZ width tends to be stable after the peak load [54, 59], despite that there may be partial microcrack closure.

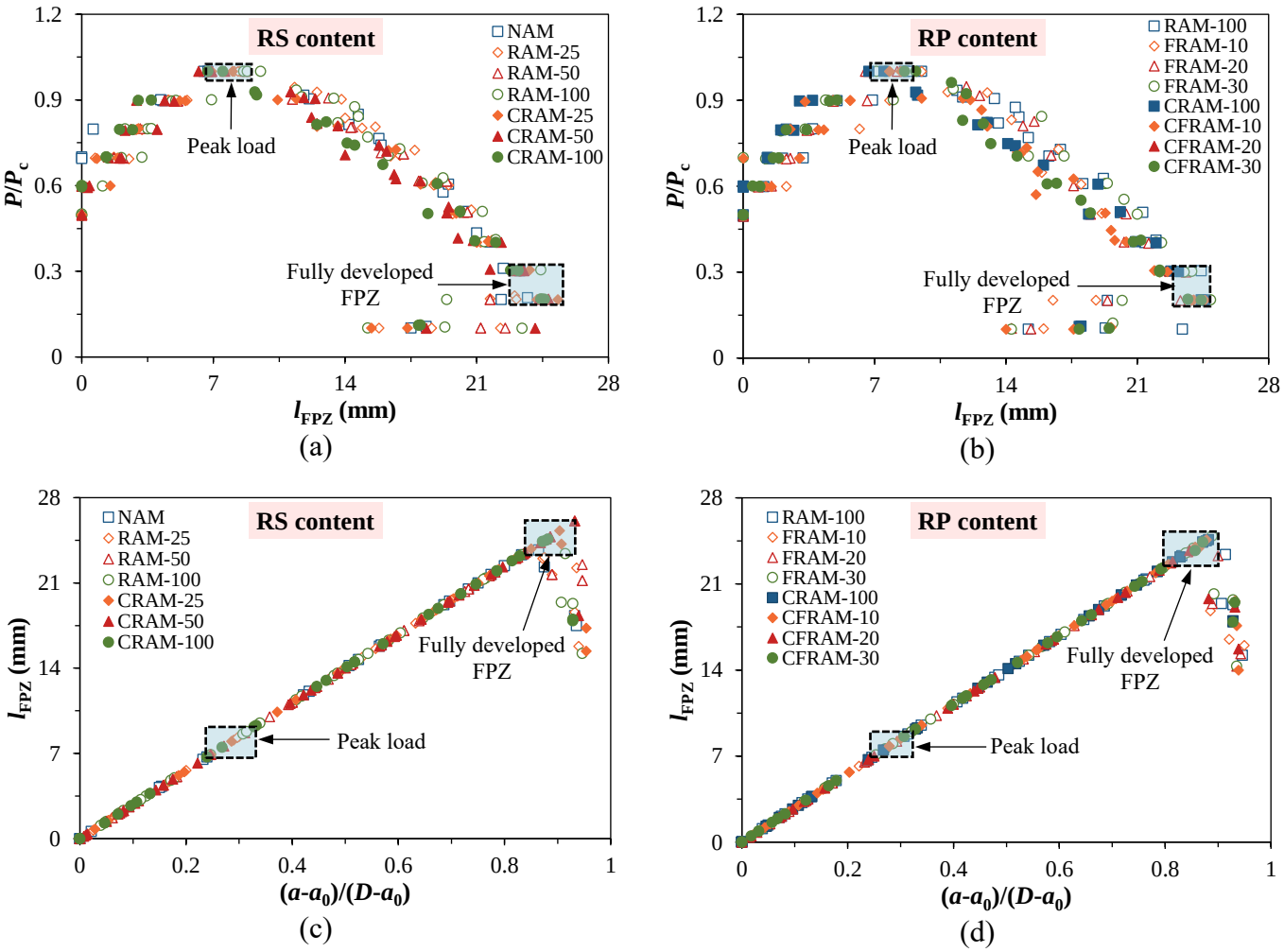

Fig. 16 The evolution of the FPZ length: (a) P/P_c versus l_{FPZ} for mortar with different RS contents; (b) P/P_c versus l_{FPZ} for mortar with different RP contents; (c) l_{FPZ} versus $(a-a_0)/(D-a_0)$ for mortar with different RS contents; (d) l_{FPZ} versus $(a-a_0)/(D-a_0)$ for mortar with different RP contents.

To compare the FPZ geometric characteristics of mortar with different recycled materials, the average fully-developed FPZ length and width of different mortars are presented in **Fig. 17**a and b, respectively. The length of FPZ remains relatively unaffected with an increase of RS/RP content while its width significantly increases when the RS content is 100%. Compared with RS, the use of RP seems to have a less significant impact on the FPZ width, except for FRAM-10. Due to the higher microporosity, the larger volume fraction of low-density C-S-H, and the lower volume fraction of hard aggregate in the mortar with RS [27], microcracks are easier to form near the main crack under external load, resulting in an increase of damage zone area. With further loading, more microcracking may be easily connected (*i.e.*, more obvious debris bridging), and thus the crack propagation resistance and energy consumption are reduced accordingly. While for the concrete using RCA, the FPZ width decreases significantly compared with normal concrete [54]. The RCA has some porous old mortar and loose old ITZ between old mortar and original aggregate, causing the crack first expanding in these weak places [70]. The fracture response of concrete seems to be

more affected by the incorporation of RCA in post-peak extension [25] which usually corresponds to the bridging action of aggregate interlock [71]. Therefore, the concrete with RCA is more prone to transgranular fracture [28] and forms more localized and intense FPZ as compared to normal concrete [23].

The results in **Fig. 17** show that, with the carbonation treatment of recycled materials, there is a slight increase in the FPZ length (about 0.8-5.6%) and a remarkable decrease in the FPZ width (about 4.4-21.8%) for recycled mortar. In an environment with appropriate relative humidity, CO_2 can react with the hydrated products and unhydrated clinker in old cement paste of recycled materials to produce high-density calcite and C-S–H gels, which is beneficial for the fill of pores, microcracks, and ITZ and reinforcement of loose particles [10, 11, 19]. As a result, for the mortar using carbonated recycled materials, the porosity is reduced, the microstructure is improved and the strength is increased [14]. Under the external loading, the spread of microcracking zone is effectively limited, resulting in a smaller fully-developed FPZ width. Whereas, the fully-developed FPZ length depends largely on the boundary conditions of the specimen, the variation in the length direction of the fully-developed FPZ is therefore extremely limited.

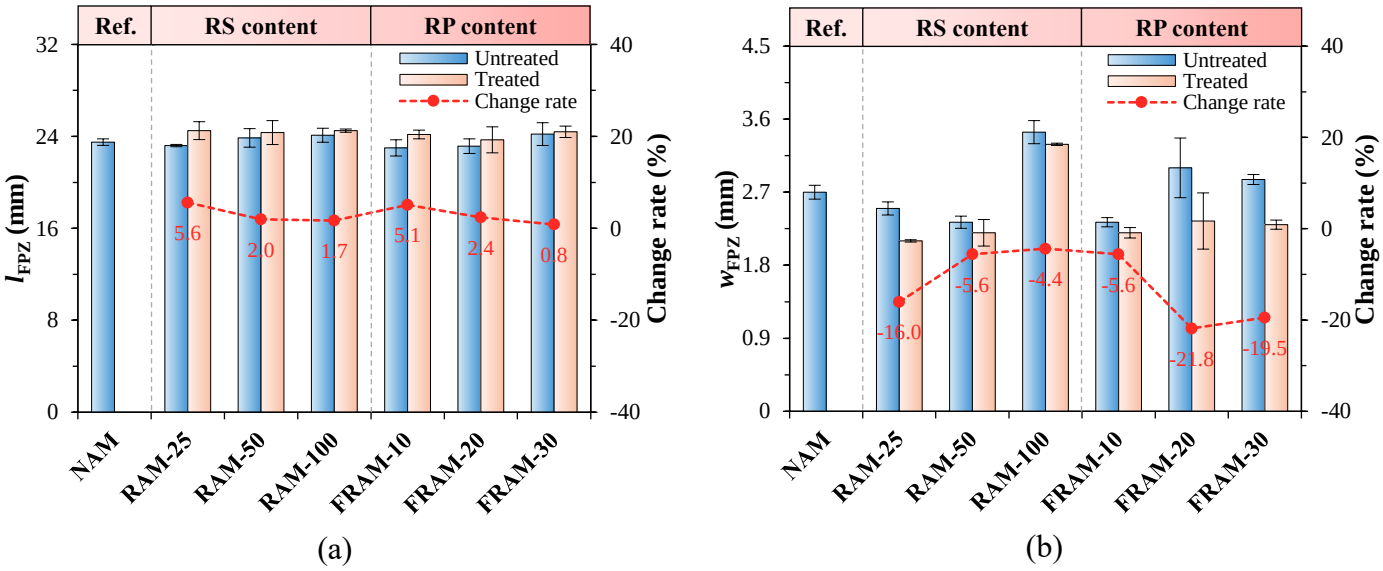

Fig. 17 The geometric characteristics of the fully-developed FPZ: (a) the FPZ length; (b) the FPZ width.

3.7. Crack extension resistance curves

Resistance curve (*R*-curve) reflecting the resistance of the material itself during crack propagation [72] is conducive to further clarify the above-mentioned possible fracture mechanism. It can be characterized in terms of stress intensity factor (K_R), energy release rate (G_R) and J-integral (J_R). Making full use of the DIC technology to measure crack lengths at various loading stages, K_R curves were adopted in this study, which were determined by putting the applied load and measured crack length into Eqs. (6) and (7).

The estimated K_R-curves of different mortars are plotted in **Fig. 17**. It can be seen from these

figures that the K_R-curves of all specimens have a similar trend of increasing with crack growth. Specifically, as the stress intensity factor at the notch tip reaches the crack initiation toughness, the crack starts to expand, and the resistance remains at a low level before the peak load, indicating the toughening mechanism during this stable crack growth stage is mainly microcracking. After the peak load, the resistance increases rapidly in the unstable crack propagation stage since debris bridging plays a dominant role in mortar. While for concrete, there may be a certain plateau segment at this stage [72], which can be attributed to the bridging effect caused by the interlock of coarse aggregates. As can be seen from **Fig. 17**a and b, with the increase of RS/CRS content, the resistance before the peak load decreases, and the reduction can be alleviated to a certain extent by CO_2 treatment. This shows that microcracking increases with the use of RS, but carbonation treatment of RS can reduce microcracking. After the peak load, the resistance reduction of RAM increases progressively with crack extension, but the employment of CO_2-treated RS decreases the reduction degree. This is consistent with the previously mentioned that the strengthening effect of carbonation treatment on mortar can cause less debris bridging. It can be noticed from Fig. 17c and d that, the utilization of RP has less influence on the resistance of the cracking process as compared to the use of RS.

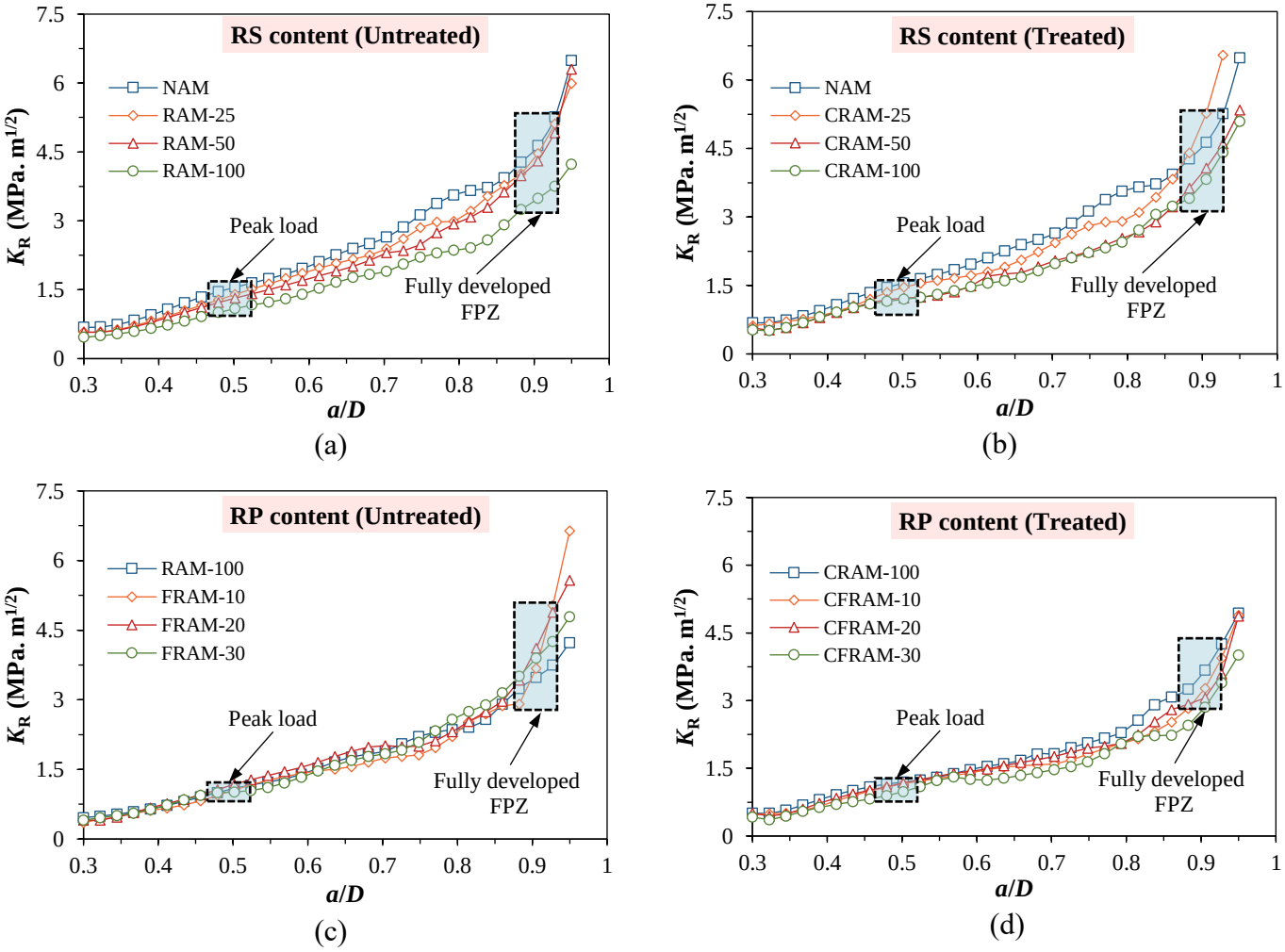

Fig. 18 K_R-curves of the mortars with different contents of RS and RP: (a) RS content (Untreated); (b) RS content (Treated); (c) RP content (Untreated); (d) RP content (Treated).

4. Low-carbon discussion

From the extracted fracture parameters and the observed crack propagation, it can be concluded that the fracture property of mortar is weakened by the addition of RS and RP, but the accelerated carbonation technology can improve it to some extent. Although the improvement effect of carbonation modification on some fracture parameters may not as good as that of ball milling [24] and acid treatment [25], it is noted that the attached mortar left by the two methods is still not effectively utilized, and the former is prone to generate additional mechanical energy consumption and carbon emissions. If the performance improvement of recycled concrete is based on the cost of additional carbon emissions, then whether it is low-carbon concrete needs further proof. Therefore, in this section, a preliminary study on the carbon emission analysis of different mortars was conducted to quantify the environmental benefits of utilizing carbonated RS and RP.

Table 3 lists the estimated embodied carbon footprint of the raw materials from the collected literatures [10, 12, 73-76]. The CO_2 emissions from grinding RS to produce RP in the lab are about 0.188–0.2457 kg/kg of RP [74]. The median value (*i.e.*, 0.217 kg CO_2 eq/kg of RP) was taken in this study. After carbonation, per kg RP can store about 0.09–0.17 kg CO_2 eq [10]. The median value (*i.e.*, 0.13 kg CO_2 eq/kg of RP) was adopted and thus the carbon emissions per kg of CRP was about 0.087 kg CO_2 eq. As per the study of Hossain *et al*. [75], the production of per kg of RS from C&D waste emits 0.012 kg CO_2 eq. Considering that the recycled concrete aggregate may sequestrate 0.0079 kg CO2 eq/kg on average [12], the carbon emissions per kg of CRS was about 0.004 kg CO_2 eq.

Table 3 Embodied carbon footprint of raw materials (kg CO_2 eq/kg).

Cement	RP	CRP	NS	RS	CRS	SP
0.931 [73]	0.217 [74]	0.087 [10, 74]	0.023 [75]	0.012 [75]	0.004 [12, 75]	1.064 [76]

By multiplying the carbon emission factors by the content of the components in **Table 2**, the carbon emissions of different mortar production can be obtained. To compare the carbon emissions of mortars with different strengths, this study adopted the CO_2 intensity [5], which was calculated by dividing the carbon emissions by the compressive strength. The determined CO_2 intensity of different mortars is illustrated in **Fig. 19**. Compared with NAM, the CO_2 intensities of untreated RAM-25 and RAM-50 are close to each other, while those of untreated RAM-100, FRAM-10, FRAM-20 and FRAM-30 are higher due to excessive strength weakening. This suggests that the carbon emissions of recycled mortar do not necessarily decrease as expected, but rather increase as the amount of recycled materials increase. It is worth mentioning that the use of recycled aggregates

reduces carbon emissions mainly by reducing transportation distances and avoiding solid waste to landfills [3], which were not considered as the environmental benefit assessment was not the focus of this study. After carbonation treatment, the CO_2 intensity of recycled mortar is reduced by about 2.0-10.8% and the reduction becomes significant when more recycled materials are incorporated. As accelerated carbonation allows for carbon sequestration while increasing strength, all mortars containing carbonated recycled materials have lower CO_2 intensity than NAM, indicating that mortars prepared with carbonated RS and RP are low-carbon cementitious materials.

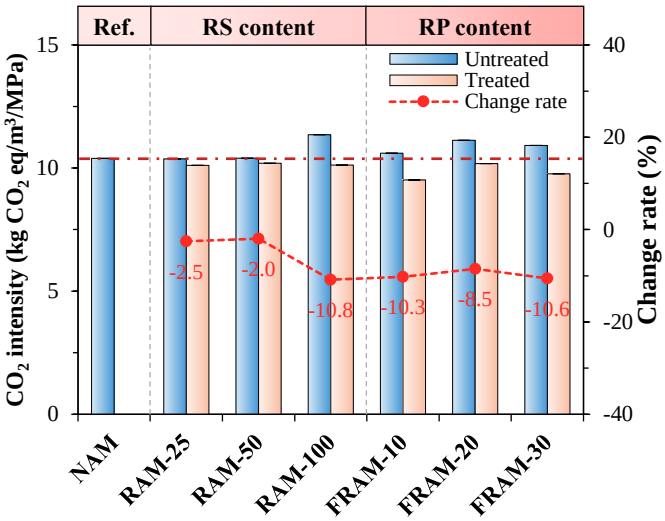

Fig. 19 CO_2 intensity of the mortars with different contents of RS and RP.

To quantify the overall effect of accelerated carbonation of recycled raw materials on the fracture characteristics of mortar, relative fracture properties were estimated by the average change rate of fracture toughness and energy as follows.

$$\text{Relative fracture properties}=\frac{1}{3}\left(\frac{K_{\text{Ic,treated}}^{\text{ini}}-K_{\text{Ic,untreated}}^{\text{ini}}}{K_{\text{Ic,untreated}}^{\text{ini}}}+\frac{K_{\text{Ic,treated}}^{\text{un}}-K_{\text{Ic,untreated}}^{\text{un}}}{K_{\text{Ic,untreated}}^{\text{un}}}+\frac{G_{\text{f,treated}}-G_{\text{f,untreated}}}{G_{\text{f,untreated}}}\right)\times 100\% \quad (9)$$

Relative carbon emissions were defined as the change rate of CO_2 intensity of recycled mortar after the carbonation treatment. **Fig. 20** shows the relative fracture properties and carbon emissions of various recycled mortars after the carbonation treatment. It is noticed that, for all mortars, the relative fracture properties are positive while the relative carbon emissions are negative, suggesting that CO_2 treatment can simultaneously improve fracture properties and reduce carbon emissions (*i.e.*, realizing synergy between safety and low carbon). The synergism increases with increasing RS content but decreases with increasing RP content. Therefore, based on the results of this study, it seems that high content of carbonated recycled sand (100%) and low content of carbonated recycled powder (10-20%) are recommended to be used in the preparation of low-carbon cementitious materials.

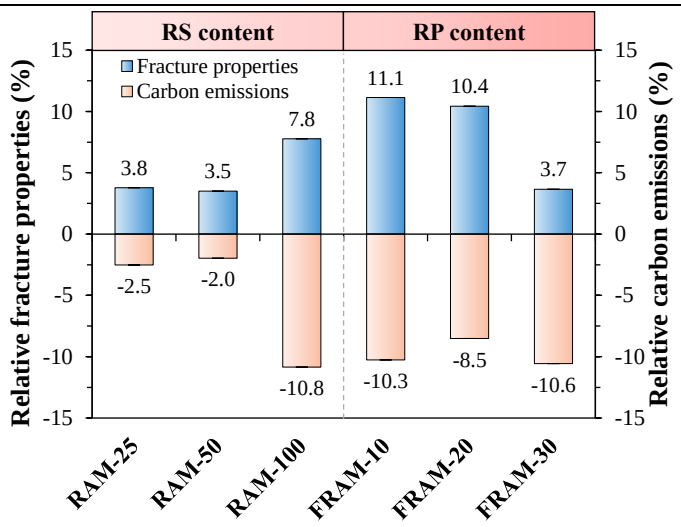

Fig. 20 Relative fracture properties and carbon emissions of the mortars with different contents of RS and RP.

5. Conclusions

Three-point bending tests were carried out on center-notched beams to study the fracture behavior of a low-carbon mortar with carbonated recycled sand and recycled powder. The effects of RS contents, RP contents and carbonation treatment on fracture parameters, crack evolution and carbon emissions of mortar were evaluated and discussed. The conclusions were drawn as follows.

(1) With the increase of RS content from 25% to 100%, the K_{Ic}^{ini} and K_{Ic}^{un} of recycled mortar decrease gradually by about 15.8-31.1% and 8.9-29.5% compared with natural mortar. When the content of RP is 10-30%, the variation of K_{Ic}^{un} of recycled mortar is relatively limited. The effect of carbonation treatment on the increase of K_{Ic}^{un} can be almost ignored, but the increase of K_{Ic}^{ini} is evident, especially at the dosage of 10-20% RP (more than 25%).

(2) The G_f values of mortar decrease with increasing RS contents (about 13.9-37.8%) while remaining steady with increasing RP contents. The improvement effect of carbonation treatment on G_f increases with the RS content (about 8.3-14.0%) and decreases with the RP content (about 5.1-7.8%).

(3) The FPZ evolution of untreated and CO_2 treated mortars exhibits similar behavior: the FPZ initiates with some microcracks and develops slowly before the peak load (about 0.24-0.32 of the ligament depth), then it expands quickly by the bridging effect and finally forms a narrow and irregular band (about 0.84-0.92 of the ligament depth) at the post-peak 0.20-0.32 of the peak load.

(4) After using RS, load-induced microcracks are easier to form near the main crack, causing an increase in the damage zone area. With further loading, more microcracking seems prone to be connected (*i.e.*, more prominent debris bridging), and thus the crack propagation resistance and energy consumption are decreased accordingly. While the use of RP mainly affects the initial

cracking stage of the cement matrix of mortar.

(5) By quantitative analysis, it is noticed that carbonation treatment can simultaneously improve fracture properties and reduce carbon emissions of cementitious materials (*i.e.*, realizing synergism of safety and low carbon). Based on the synergistic effect of this study, it is recommended to use high contents of carbonated RS (100%) and low contents of carbonated RP (10-20%) in the preparation of low-carbon mortars.

Acknowledgements

The financial support from the National Natural Science Foundation of China (No. 52078358, 52208284) and National Key R&D Program of China (2022YFC3803400, 2022YFE0198300) is gratefully appreciated.

References

[1] X. Zhao, X. Ma, B. Chen, Y. Shang, M. Song, Challenges toward carbon neutrality in China: Strategies and countermeasures, Resources, Conservation and Recycling 176 (2022) 105959.

[2] CABEE, China Building Energy Consumption Annual Report 2020, BUILDING ENERGY EFFICIENCY 49(02) (2021) 1-6.

[3] Y. Tang, J. Xiao, Q. Liu, B. Xia, A. Singh, Z. Lv, W. Song, Natural gravel-recycled aggregate concrete applied in rural highway pavement: Material properties and life cycle assessment, Journal of Cleaner Production 334 (2022) 130219.

[4] J. Xiao, Recycled Aggregate Concrete Structures, Springer Berlin, Heidelberg, 2018.

[5] J. Xiao, H. Zhang, Y. Tang, Q. Deng, D. Wang, C.-s. Poon, Fully utilizing carbonated recycled aggregates in concrete: Strength, drying shrinkage and carbon emissions analysis, Journal of Cleaner Production 377 (2022) 134520.

[6] A. Mistri, N. Dhami, S.K. Bhattacharyya, S.V. Barai, A. Mukherjee, W.K. Biswas, Environmental implications of the use of bio-cement treated recycled aggregate in concrete, Resour Conserv Recy 167 (2021) 105436.

[7] K. Ouyang, C. Shi, H. Chu, H. Guo, B. Song, Y. Ding, X. Guan, J. Zhu, H. Zhang, Y. Wang, J. Zheng, An overview on the efficiency of different pretreatment techniques for recycled concrete aggregate, Journal of Cleaner Production 263 (2020) 121264.

[8] Q. Tang, Z.M. Ma, H.X. Wu, W. Wang, The utilization of eco-friendly recycled powder from concrete and brick waste in new concrete: A critical review, Cement Concrete Comp 114 (2020) 103807.

[9] V.W.Y. Tam, A. Butera, K.N. Le, W.G. Li, Utilising CO2 technologies for recycled aggregate concrete: A critical review, Construction and Building Materials 250 (2020) 118903.

[10] Y. Zhang, H. Chen, Q. Wang, Accelerated carbonation of regenerated cementitious materials from waste concrete for CO2 sequestration, Journal of Building Engineering 55 (2022) 104701.

[11] J. Zhang, C. Shi, Y. Li, X. Pan, C.-S. Poon, Z. Xie, Influence of carbonated recycled concrete aggregate on properties of cement mortar, Construction and Building Materials 98 (2015) 1-7.

[12] D. Xuan, B. Zhan, C.S. Poon, Assessment of mechanical properties of concrete incorporating carbonated recycled concrete aggregates, Cement and Concrete Composites 65 (2016)

67-74.

[13] D. Xuan, B. Zhan, C.S. Poon, Durability of recycled aggregate concrete prepared with carbonated recycled concrete aggregates, Cement and Concrete Composites 84 (2017) 214-221.

[14] B.J. Zhan, D.X. Xuan, C.S. Poon, K.L. Scrivener, Characterization of interfacial transition zone in concrete prepared with carbonated modeled recycled concrete aggregates, Cement and Concrete Research 136 (2020) 106175.

[15] S. Luo, S. Ye, J. Xiao, J. Zheng, Y. Zhu, Carbonated recycled coarse aggregate and uniaxial compressive stress-strain relation of recycled aggregate concrete, Construction and Building Materials 188 (2018) 956-965.

[16] L. Li, C.S. Poon, J. Xiao, D. Xuan, Effect of carbonated recycled coarse aggregate on the dynamic compressive behavior of recycled aggregate concrete, Construction and Building Materials 151 (2017) 52-62.

[17] C. Liang, H. Ma, Y. Pan, Z. Ma, Z. Duan, Z. He, Chloride permeability and the caused steel corrosion in the concrete with carbonated recycled aggregate, Construction and Building Materials 218 (2019) 506-518.

[18] L. Peng, W. Zeng, Y. Zhao, L. Li, C.-s. Poon, H. Zheng, Steel corrosion and corrosion-induced cracking in reinforced concrete with carbonated recycled aggregate, Cement and Concrete Composites 133 (2022) 104694.

[19] B. Lu, C. Shi, J. Zhang, J. Wang, Effects of carbonated hardened cement paste powder on hydration and microstructure of Portland cement, Construction and Building Materials 186 (2018) 699-708.

[20] S.P. Shah, S.E. Swartz, C. Ouyang, Fracture Mechanics of Concrete: Applications of Fracture Mechanics to Concrete, Rock and Other Quasi-Brittle Materials, John Wiley & Sons, Inc., New York, 1995.

[21] E. Ghorbel, G. Wardeh, Influence of recycled coarse aggregates incorporation on the fracture properties of concrete, Construction and Building Materials 154 (2017) 51-60.

[22] T. Li, J. Xiao, Y. Zhang, B. Chen, Fracture behavior of recycled aggregate concrete under three-point bending, Cement and Concrete Composites 104 (2019) 103353.

[23] M. Guo, S.Y. Alam, A.Z. Bendimerad, F. Grondin, E. Rozière, A. Loukili, Fracture process zone characteristics and identification of the micro-fracture phases in recycled concrete, Engineering Fracture Mechanics 181 (2017) 101-115.

[24] H. Dilbas, O. Cakir, H. Yildirim, An experimental investigation on fracture parameters of recycled aggregate concrete with optimized ball milling method, Construction and Building Materials 252 (2020) 119118.

[25] F. Kazemian, H. Rooholamini, A. Hassani, Mechanical and fracture properties of concrete containing treated and untreated recycled concrete aggregates, Construction and Building Materials 209 (2019) 690-700.

[26] S. Pradhan, S. Kumar, S.V. Barai, Impact of particle packing mix design method on fracture properties of natural and recycled aggregate concrete, Fatigue Fract Eng M 42(4) (2019) 943-958.

[27] A.T. Akono, J.X. Chen, M.M. Zhan, S.P. Shah, Basic creep and fracture response of fine recycled aggregate concrete, Construction and Building Materials 266 (2021) 121107.

[28] J. Xiao, Y. Tang, H. Chen, H. Zhang, B. Xia, Effects of recycled aggregate combinations and recycled powder contents on fracture behavior of fully recycled aggregate concrete, Journal of

Cleaner Production 366 (2022) 132895.

[29] GB/T 25176-2010, Recycled fine aggregate for concrete and mortar, National Standard of the People's Republic of China.

[30] GB/T 14684-2011, Sand for construction, National Standard of the People's Republic of China.

[31] BS EN 1097-6, Tests for mechanical and physical properties of aggregates, in: BS EN 1097-6 (Ed.) Determination of particle density and water absorption, British Standard, 2000.

[32] Z.H. Duan, S.D. Hou, J.Z. Xiao, B. Li, Study on the essential properties of recycled powders from construction and demolition waste, Journal of Cleaner Production 253 (2020) 119865.

[33] M.E. Sosa, Y.A. Villagrán Zaccardi, C.J. Zega, A critical review of the resulting effective water-to-cement ratio of fine recycled aggregate concrete, Construction and Building Materials 313 (2021) 125536.

[34] P. Plaza, I.F.S. del Bosque, M. Frias, M.I.S. de Rojas, C. Medina, Use of recycled coarse and fine aggregates in structural eco-concretes. Physical and mechanical properties and CO2 emissions, Construction and Building Materials 285 (2021) 122926.

[35] Y. Tang, J. Xiao, H. Zhang, Z. Duan, B. Xia, Mechanical properties and uniaxial compressive stress-strain behavior of fully recycled aggregate concrete, Construction and Building Materials 323 (2022) 126546.

[36] V.W.Y. Tam, C.M. Tam, Y. Wang, Optimization on proportion for recycled aggregate in concrete using two-stage mixing approach, Construction and Building Materials 21(10) (2007) 1928-1939.

[37] GB/T 50081-2019, Standard for test methods of concrete physical and mechanical properties, National Standard of the People's Republic of China.

[38] ASTM C511-21, Standard Specification for Mixing Rooms, Moist Cabinets, Moist Rooms, and Water Storage Tanks Used in the Testing of Hydraulic Cements and Concretes, American Society for Testing and Materials.

[39] BS 1881-117, Method for determination of tensile splitting strength, British Standard, 1983.

[40] S.L. Xu, Q.H. Li, Y. Wu, L.X. Dong, Y. Lyu, H.W. Reinhardt, C.K.Y. Leung, G. Ruiz, S. Kumar, S.W. Hu, RILEM Standard: testing methods for determination of the double-K criterion for crack propagation in concrete using wedge-splitting tests and three-point bending beam tests, recommendation of RILEM TC265-TDK, Materials and Structures 54(6) (2021) 220.

[41] Q.F. Liu, D.T.W. Looi, H.H. Chen, C. Tang, R.K.L. Su, Framework to optimise two-dimensional DIC measurements at different orders of accuracy for concrete structures, Structures 28 (2020) 93-105.

[42] R. Kumar, S.C.B. Gurram, A.K. Minocha, Influence of recycled fine aggregate on microstructure and hardened properties of concrete, Magazine of Concrete Research 69(24) (2017) 1288-1295.

[43] Y.-J. Kim, Quality properties of self-consolidating concrete mixed with waste concrete powder, Construction and Building Materials 135 (2017) 177-185.

[44] M. Nedeljkovic, J. Visser, B. Savija, S. Valcke, E. Schlangen, Use of fine recycled concrete aggregates in concrete: A critical review, Journal of Building Engineering 38 (2021) 102196.

[45] H. Zhang, T. Ji, X. Zeng, Z. Yang, X. Lin, Y. Liang, Mechanical behavior of ultra-high performance concrete (UHPC) using recycled fine aggregate cured under different conditions and

the mechanism based on integrated microstructural parameters, Construction and Building Materials 192 (2018) 489-507.

[46] J. Wang, J. Zhang, D. Cao, H. Dang, B. Ding, Comparison of recycled aggregate treatment methods on the performance for recycled concrete, Construction and Building Materials 234 (2020) 117366.

[47] Y.S. Jenq, S.P. Shah, Two parameter fracture model for concrete, J Eng Mech 111(10) (1985) 1227-1241.

[48] S.L. Xu, H.W. Reinhardt, Determination of double-K criterion for crack propagation in quasi-brittle fracture, Part I: Experimental investigation of crack propagation, Int J Fracture 98(2) (1999) 111-149.

[49] S. Khalilpour, E. BaniAsad, M. Dehestani, A review on concrete fracture energy and effective parameters, Cement and Concrete Research 120 (2019) 294-321.

[50] RILEM, TC 50-FMC Fracture Mechanics of Concrete, Determination of the Fracture Energy of Mortar and Concrete by Means of Three-point Bend Tests on Notched Beams, Materials and Structures 18(4) (1985) 287-290.

[51] W. Chen, L.X. Peng, H.F. Yang, Fracture behaviors of concrete incorporating different levels of recycled coarse aggregate after exposure to elevated temperatures, Journal of Building Engineering 35 (2021) 102040.

[52] H.H. Chen, R.K.L. Su, Tension softening curves of plain concrete, Construction and Building Materials 44 (2013) 440-451.

[53] Z.M. Wu, H. Rong, J.J. Zheng, F. Xu, W. Dong, An experimental investigation on the FPZ properties in concrete using digital image correlation technique, Engineering Fracture Mechanics 78 (2011) 2978–2990.

[54] Y. Xu, H. Chen, Y. Tang, Study on fracture parameters and fracture process zone of manufactured-sand recycled aggregate concrete, Construction and Building Materials 361 (2022) 129613.

[55] Y. Tang, H. Chen, J. Xiao, Size effects on the characteristics of fracture process zone of plain concrete under three-point bending, Construction and Building Materials 315 (2021) 125725.

[56] Y.X. Tang, R.K.L. Su, H.N. Chen, Characterization on tensile behaviors of fracture process zone of nuclear graphite using a hybrid numerical and experimental approach, Carbon 155 (2019) 531-544.

[57] Y. Tang, H. Chen, Characterizations on fracture process zone of plain concrete, J Civ Eng Manag 25 (2019) 819-830.

[58] CEB, CEB-FIP Model Code 1990, CEB Bulletin D'information 195 (1990).

[59] S. Das, M. Aguayo, G. Sant, B. Mobasher, N. Neithalath, Fracture process zone and tensile behavior of blended binders containing limestone powder, Cement and Concrete Research 73 (2015) 51-62.

[60] S. Das, M. Aguayo, V. Dey, R. Kachala, B. Mobasher, G. Sant, N. Neithalath, The fracture response of blended formulations containing limestone powder: Evaluations using two-parameter fracture model and digital image correlation, Cement Concrete Comp 53 (2014) 316-326.

[61] S. Das, A. Kizilkanat, N. Neithalath, Crack propagation and strain localization in metallic particulate-reinforced cementitious mortars, Mater Design 79 (2015) 15-25.

[62] Y.X. Tang, R.K.L. Su, H.N. Chen, Energy dissipation during fracturing process of nuclear graphite based on cohesive crack model, Engineering Fracture Mechanics 242 (2021) 107426.

[63] A. Hillerborg, M. Modéer, P.E. Petersson, Analysis of crack formation and crack growth in concrete by means of fracture mechanics and finite elements Cement and Concrete Research 6(6) (1976) 773-781

[64] R.K.L. Su, H.H.N. Chen, A.K.H. Kwan, Incremental displacement collocation method for the evaluation of tension softening curve of mortar, Engineering Fracture Mechanics 88 (2012) 49-62.

[65] H.H.N. Chen, R.K.L. Su, S.L. Fok, H.G. Zhang, Fracture behavior of nuclear graphite under three-point bending tests, Engineering Fracture Mechanics 186 (2017) 143-157.

[66] R.K.L. Su, H.H. Chen, S.L. Fok, H. Li, G. Singh, L. Sun, L. Shi, Determination of the tension softening curve of nuclear graphites using the incremental displacement collocation method, Carbon 57 (2013) 65-78.

[67] P.E. Petersson, Crack growth and development of fracture zones in plain concrete and similar materials Report No. TVBM 1006, Division of Building Materials, LTH, Lund university (1981).

[68] X.Z. Hu, K. Duan, Influence of fracture process zone height on fracture energy of concrete, Cement and Concrete Research 34(8) (2004) 1321-1330.

[69] X. Hu, Q. Li, Z. Wu, S. Yang, Modelling fracture process zone width and length for quasi-brittle fracture of rock, concrete and ceramics, Engineering Fracture Mechanics 259 (2022) 108158.

[70] J. Xiao, Q. Liu, Y.C. Wu, Numerical and experimental studies on fracture process of recycled concrete, Fatigue Fract Eng M 35(8) (2012) 801-808.

[71] N. Nomura, H. Mihashi, M. Izumi, Correlation of Fracture Process Zone and Tension Softening Behavior in Concrete, Cement and Concrete Research 21(4) (1991) 545-550.

[72] S. Xu, H.W. Reinhardt, Crack Extension Resistance and Fracture Properties of Quasi-Brittle Softening Materials like Concrete Based on the Complete Process of Fracture, Int J Fracture 92(1) (1998) 71-99.

[73] K.-H. Yang, Y.-B. Jung, M.-S. Cho, S.-H. Tae, Effect of supplementary cementitious materials on reduction of CO2 emissions from concrete, Journal of Cleaner Production 103 (2015) 774-783.

[74] L. Likes, A. Markandeya, M.M. Haider, D. Bollinger, J.S. McCloy, S. Nassiri, Recycled concrete and brick powders as supplements to Portland cement for more sustainable concrete, Journal of Cleaner Production (2022) 132651.

[75] M.U. Hossain, C.S. Poon, I.M.C. Lo, J.C.P. Cheng, Comparative environmental evaluation of aggregate production from recycled waste materials and virgin sources by LCA, Resources, Conservation and Recycling 109 (2016) 67-77.

[76] A. Sahraei Moghadam, F. Omidinasab, S. Moazami Goodarzi, Characterization of concrete containing RCA and GGBFS: Mechanical, microstructural and environmental properties, Construction and Building Materials 289 (2021) 123134.